

**OXPHOS deficiencies affect peroxisome proliferation by downregulating genes controlled by the SNF1 signaling pathway**

Jean-Claude Farré\*, Krypton Carolino, Lou Devanneaux, Suresh Subramani\*

*Section of Molecular Biology, Division of Biological Sciences, University of California, San Diego, La Jolla, CA 92093-0322, USA*

\*Correspondence to Jean-Claude Farré [jfarre@ucsd.edu](mailto:jfarre@ucsd.edu) or Suresh Subramani [ssubramani@ucsd.edu](mailto:ssubramani@ucsd.edu), Section of Molecular Biology, Division of Biological Sciences, University of California, San Diego, La Jolla, CA 92093-0322, USA

**Running Title:** Interplay between mitochondrial OXPHOS and peroxisome proliferation

**Keywords:** Peroxisome, mitochondria, OXPHOS, SNF1, Gal83, peroxisome proliferation

**Summary**

How environmental cues influence peroxisome proliferation, particularly through organelles, remains largely unknown. Yeast peroxisomes metabolize fatty acids (FA), and methylotrophic yeasts also metabolize methanol. NADH and acetyl-CoA, produced by these pathways enter mitochondria for ATP production and for anabolic reactions. During the metabolism of FA and/or methanol, the mitochondrial oxidative phosphorylation (OXPHOS) pathway accepts NADH for ATP production and maintains cellular redox balance. Remarkably, peroxisome proliferation in *Pichia pastoris* was abolished in NADH shuttling- and OXPHOS mutants affecting complex I or III, or by the mitochondrial uncoupler, 2,4-dinitrophenol (DNP),

indicating ATP depletion causes the phenotype. We show that mitochondrial OXPHOS deficiency inhibits expression of several peroxisomal proteins implicated in FA and methanol metabolism, as well as in peroxisome division and proliferation. These genes are regulated by the Snf1 complex (SNF1), a pathway generally activated by a high AMP/ATP ratio. In OXPHOS mutants, Snf1 is activated by phosphorylation, but Gal83, its interacting subunit, fails to translocate to the nucleus. Phenotypic defects in peroxisome proliferation observed in the OXPHOS mutants, and phenocopied by the  $\Delta gal83$  mutant, were rescued by deletion of three transcriptional repressor genes (*MIG1*, *MIG2* and *NRG1*) controlled by SNF1 signaling. Our results are interpreted in terms of a mechanism by which peroxisomal and mitochondrial proteins and/or metabolites influence redox and energy metabolism, while also influencing peroxisome biogenesis and proliferation, thereby exemplifying interorganellar communication and interplay involving peroxisomes, mitochondria, cytosol and the nucleus. We discuss the physiological relevance of this work in the context of human OXPHOS deficiencies.

## Introduction

Like other subcellular organelles, peroxisomes divide and segregate to endow daughter cells with peroxisomes. Cells stringently regulate organelle number, volume, size and content in response to environmental signals. Regulation of these properties, together with organelle dynamics and homeostasis, allows cells to endure metabolic or environmental stress, cope with the needs of cell division or differentiation, remove excess or damaged organelles by turnover, correct imbalances in organelle segregation during cell division or repopulate organelles with different enzymes upon switching to a new environment. The division of some organelles, such as the nucleus or the Golgi apparatus, is coupled to the cell cycle [1]. However, for others, such as mitochondria and chloroplasts, division is uncoupled from cell division [2]. Peroxisomes division can be coupled or uncoupled from cell division [3]. The de-coupling of peroxisome division during the cell-cycle and cell division is likely due to the ability of cells to also produce peroxisomes *de novo* [4].

In yeast and other eukaryotes, three major pathways control peroxisome number. First, in constitutively-dividing cells, peroxisomes divide by fission of pre-existing peroxisomes, a process we refer to simply as peroxisome division [5, 6]. This process regulates peroxisome number in a geometric manner. A second pathway is where peroxisomes are induced to create many new organelles exponentially, a process we call ‘peroxisome proliferation’. Finally, peroxisome number is also controlled by pexophagy, the selective degradation of peroxisome by autophagic processes [7].

In yeasts, peroxisome division occurs both during constitutive growth and cell division. Peroxisome size and number are sensitive to peroxisomal metabolic pathways and the metabolites available [8-11]. Changes in peroxisome number and size can also be induced by

peroxisome proliferation, which generally occurs when cells are shifted to nutrients whose metabolism requires peroxisomes and their enzymes [6, 12]. Finally, peroxisomal contents can also vary depending on the growth media whose metabolism requires different peroxisomal enzymes [6].

Peroxisome division uses a machinery also required for mitochondrial fission [13]. In yeast, this machinery is comprised of the proteins Fis1, Mdv and Caf4, as well as the dynamin-related GTPase, Dnm1 [14, 15]. The Pex11 family of proteins activates peroxisome division specifically [16-18]. These proteins are conserved in evolution [13, 19] and are responsible for diseases in humans and plants [20-22]. In *Saccharomyces cerevisiae*, while Pex11 promotes the division of peroxisomes already present in the cell, Pex25 initiates remodeling at the peroxisomal membrane to allow proliferation and Pex27 counters this activity [16].

Our current understanding of the mechanisms by which environmental cues activate peroxisome proliferation is rather limited [11, 19, 23, 24]. In *S. cerevisiae*, peroxisome proliferation coincides with the transcriptional regulation, by non-fermentable oleate, of SNF1 complex-mediated induction of several peroxisomal  $\beta$ -oxidation and peroxisome proliferation genes [25-28]. The Snf1 protein - the ortholog of the mammalian AMP-activated protein kinase (AMPK) - is a heterotrimer of the Snf1 catalytic subunit, the Snf4 activation subunit [29], and one of three  $\beta$  subunits (Sip1, Sip2, and Gal83) that localize the SNF1 complex to different cellular compartments [29, 30]. Gal83 directs the SNF1 complex to the nucleus in a glucose-regulated manner and facilitates the physical interaction between SNF1 and nuclear transcription factors [31]. In yeast cells grown in the absence of glucose, Snf1 is active via phosphorylation within its activation loop at Thr210 (T210) primarily by Sak1, but also by Tos3 and Elm1 [32-34]. The activated SNF1 complex inactivates the transcriptional repressors, Mig1 and Mig2 [35],



via their phosphorylation [36, 37] and export from the nucleus, thereby enabling activation by the transcriptional activator, Adr1 [38].

Two additional transcriptional activators, Oaf1 and Pip2, regulate genes in response to oleate induction conditions [23, 27]. However, these transcription activators have not been described in *P. pastoris* (now reclassified as *Komagataella phaffii*) [39].

In contrast, the addition of glucose to cells (glucose repression) results in a reduction in ADP levels that causes the Glc7-Reg1 protein phosphatase to dephosphorylate T210 and thereby inactivate Snf1 [40-42].

Notably, this entire description of peroxisome induction and proliferation involves transactions of proteins and metabolites residing in three compartments – the cytosol, nucleus and peroxisomes, with no direct involvement of mitochondria. Yet, it is clear that peroxisomes contact other subcellular compartments, including mitochondria [43-45]. Furthermore, mutations in genes affecting peroxisome biogenesis also impair mitochondrial function and morphology [46, 47], and the reverse is also true [48].

We probed more deeply into the regulation of peroxisome content and proliferation in *P. pastoris*. During growth in glucose, most *P. pastoris* cells possess a few, small peroxisomes, with a limited luminal content, but when cells are grown in oleate, numerous, small peroxisomes proliferate and are distributed throughout the cells, whereas in methanol medium the peroxisomes are large, less numerous, and clustered [49].

We reveal here the mechanism and players involved in the important interorganellar interplay involving the cytosol, nucleus, peroxisomes and mitochondria by which peroxisomal and mitochondrial metabolites influence redox and energy metabolism in the two compartments, while also influencing peroxisome biogenesis and proliferation.

## Results

### Peroxisome proteins/metabolites influence peroxisome size

We reinvestigated whether peroxisomal metabolites influence peroxisome size and number in *P. pastoris*. Peroxisomes were labelled with the functional, fluorescently-tagged, peroxisomal membrane proteins (PMPs), Pex3-GFP or GFP-Pex36, in several mutant strains grown in different carbon sources (Fig. 1). We deleted key genes encoding enzymes of the FA  $\beta$ -oxidation and methanol metabolism pathways, as well as a peroxin required for the import of peroxisome matrix proteins. Supporting previous findings, wherein intermediates of peroxisome metabolism, or the absence of certain peroxisomal enzymes, regulate the maturation and fission of the organelle [50, 51], the lack of 3-ketoacyl-CoA thiolase (Pot1), an enzyme responsible for the last step of FA  $\beta$ -oxidation, affected peroxisome proliferation exclusively in oleate (Fig. 1, figure supplement 1). Similarly, the lack of alcohol oxidase (Aox) 1 and 2, the first enzymes in the methanol utilization pathway (MUT), affected peroxisome proliferation only in cells grown in methanol medium (Fig. 1, figure supplement 1). Similarly, the lack of Pex5, responsible for the import of PTS1-containing enzymes (including some involved in the  $\beta$ -oxidation and MUT pathways), impaired peroxisome proliferation in both media (Fig. 1, figure supplement 1). These results show that one or more peroxisomal intermediate metabolite/s induces peroxisome proliferation, in addition to previous reports regarding their effects on division.

The molecular target of the signaling pathway that triggers peroxisome proliferation has not yet been elucidated. We hypothesized that if peroxisomal proteins/metabolites regulate proliferation, they must communicate with the cytosol and/or other organelles to induce the lipid and membrane transfer needed for peroxisome growth [52, 53]. Additionally, there must be activation of the fission machinery needed to increase peroxisome numbers [16].

In *S. cerevisiae*, the final intraperoxisomal products of  $\beta$ -oxidation are NADH and acetyl-CoA, for cells grown in FA (Fig. 1B, [54]). The transport of reducing equivalents out of peroxisomes and the maintenance of the intraperoxisomal redox balance in *S. cerevisiae* is mediated by the malate/oxaloacetate shuttle during growth in oleate, and by both the malate/oxaloacetate and the glycerol-3-phosphate/dihydroxyacetone phosphate (G3P/DHAP) shuttles, during growth in glucose [55]. The malate/oxaloacetate shuttle is coordinated by three  $\text{NAD}^+$ -dependent malate dehydrogenases: the mitochondrial Mdh1 that is part of the TCA cycle, the peroxisomal Mdh3 which regenerates  $\text{NAD}^+$  for FA  $\beta$ -oxidation, and cytosolic Mdh2, probably involved in the glyoxylate cycle [56]. The G3P/DHAP shuttle is coordinated by two G3P dehydrogenases: the mitochondrial Gpd2 and peroxisomal/cytosolic Gpd1 [57, 58]. *P. pastoris* possesses only two malate dehydrogenases (designated MdhA or B) and one G3P dehydrogenase (GpdA). We recently reported that MdhA and GpdA are predominantly mitochondrial enzymes in all media analyzed, whereas MdhB is cytosolic during growth in glucose or methanol, but is cytosolic/peroxisomal during growth in oleate [59]. The transport of acetyl-CoA from the peroxisome to the mitochondria uses two pathways [60]. The first involves peroxisomal conversion of acetyl-CoA into citrate by peroxisomal citrate synthase (Cit2), followed by citrate transport to mitochondria. The second pathway involves peroxisomal conversion of acetyl-CoA into acetylcarnitine by carnitine transferase (Cat2), which is then transported to mitochondria.

With the intent of blocking the shuttling of NADH and acetyl-CoA to the mitochondria, we made single and double deletions of components of both NADH shuttles, and the *CAT2* gene in *P. pastoris* and analyzed peroxisome status after 24 h of induction in oleate medium using Pex3-GFP and BFP appended with a PTS1 (BFP-SKL) (Fig. 1C, 1E). We observed no, or partial,

peroxisome defects in the single NADH-shuttle mutants (Fig. 1, figure supplement 2). Interestingly, in both double deletion strains,  $\Delta gpdA \Delta mdhA$  and  $\Delta gpdA \Delta mdhB$ , as well as  $\Delta cat2$ , most of the cells grown in oleate contained only a single, import-competent peroxisome (Fig. 1C). The results for the NADH-shuttling mutants are consistent with their role in maintaining the intraperoxisomal redox balance and peroxisome proliferation during growth in oleate, but surprisingly the lack of Cat2, not directly implicated in redox balance, had a similar peroxisome proliferation defect.

As a methylotrophic yeast, *P. pastoris* uses methanol as a sole carbon source for carbon assimilation and energy production (Fig. 1B). Peroxisomes are directly involved in methanol metabolism and similarly to oleate, methanol induces peroxisome proliferation. Methanol is metabolized to formaldehyde, which diffuses to the cytosol and is oxidized by a dehydrogenase (Fld1) to formate, which is further oxidized by a second dehydrogenase (Fdh1) to carbon dioxide, yielding NADH. This NADH then shuttles to the mitochondria to maintain the cytosolic redox balance and to feed mitochondrial OXPHOS. We analyzed the same yeast strains from Fig. 1C and 1E in methanol and unexpectedly, we found the same peroxisome proliferation defects observed for oleate cultures (Fig. 1D and 1F). The phenotypes of the NADH-shuttling mutants during growth in methanol are relevant because the redox reactions in this medium happen in the cytosol. Moreover, no major role of Cat2 during methanol metabolism was expected, but it might be feeding intermediates of methanol metabolism into the TCA cycle (Fig. 1B) [61].

The similar phenotypes of the NADH-shuttling and *cat2* mutants in both media suggest that redox imbalance is not the main reason for peroxisome proliferation defects, but rather could

be due to the absence of a molecule common to both pathways (NADH- and acetyl-CoA-shuttling pathways).

### **Mitochondrial OXPHOS mutants also affect multiple peroxisome phenotypes**

We hypothesized that NADH, which shuttles to the mitochondria during growth in methanol medium, or produced by the TCA cycle from peroxisomal metabolites, could trigger peroxisome proliferation. In *P. pastoris*, the NADH shuttled to the mitochondria is oxidized by the respiratory chain. The NADH dehydrogenase complex I (CI) is the main entry point for electrons into the respiratory chain. It directly oxidizes NADH to  $\text{NAD}^+$  and concomitantly reduces coenzyme Q (CoQ, ubiquinone), which causes  $\text{H}^+$  to be pumped out across the inner mitochondrial membrane, to contribute to the proton gradient that drives ATP synthesis [62].

To study the involvement of mitochondrial NADH oxidation in peroxisome proliferation and fission, we deleted two, nuclear-encoded genes encoding the mitochondrial complex I, the accessory subunit, Ndufa9, and the core subunit, NugM [62]. Because none of these mutants have been previously characterized in *P. pastoris*, we confirmed their necessity for the electron transport chain in response to metabolic substrates using Biolog's Yeast Mitochondrial Energy Substrate Assays (Fig. 2, figure supplement 1).

Furthermore, as seen for NADH- and acetyl-CoA-shuttling mutants, we observed no increase in peroxisome number or size in either CI mutant in both media (Fig. 2).

To differentiate a direct role of CI in peroxisome proliferation from the general role of electron transfer and proton translocation, we deleted a gene (*CYT1*, encoding a core subunit of CIII) encoding a downstream component of the OXPHOS complex, but not directly implicated in NADH oxidation. Like the CI mutants, the  $\Delta\text{cyt1}$  mutant also blocked peroxisome

proliferation in both media (Fig. 2), indicating that peroxisome proliferation depends on a functional mitochondrial respiratory chain.

The similarity in peroxisome proliferation defects between mutants of CI and CIII suggested that the lack of ATP synthesis, and not the reduction of NADH, causes these phenotypes. To verify this hypothesis, we used the mitochondrial uncoupler, DNP, which separates the flow of electrons from the pumping of H<sup>+</sup> ions for ATP synthesis [63]. We followed peroxisome proliferation in methanol after 3 and 24 h, using WT cells expressing Pex3-GFP (Fig. 3) and found that DNP fully abolished peroxisome proliferation, confirming that ATP synthesis is necessary for peroxisome proliferation.

### **The OXPHOS effect on peroxisome proliferation acts via the Snf1 kinase pathway in *P. pastoris***

Due to the lack of peroxisome proliferation, we checked the relative protein abundance of the key peroxisome division factor, Pex11 (Pex11-2HA expressed from its own promoter, P<sub>PEX11</sub>) after 4 h of induction in oleate medium (Fig. 4A). Remarkably, we did not detect Pex11-2HA in  $\Delta$ nugM cells, suggesting that an inactive SNF1 pathway could explain the OXPHOS deficiency. In *S. cerevisiae*, the proliferative capacity of peroxisomes coincides with the FA-responsive transcriptional regulation of many genes encoding peroxisomal proteins, including Pex11 [64]. Many such genes are repressed in glucose [65, 66] and derepressed in oleate [67] in a manner that depends on the SNF1 signaling pathway.

In *P. pastoris*, the regulation of peroxisomal genes involved in  $\beta$ -oxidation has not been studied much. However, many studies have focused on the regulation of the AOX1 promoter (P<sub>AOX1</sub>) during growth in glucose, glycerol and methanol media [68-71]. Similar to  $\beta$ -oxidation genes, AOX1

is repressed during growth in glucose and strongly induced by methanol. The transcriptional activator, Mxr1 (which shares sequence and functional homology with *S. cerevisiae* Adr1) [71, 72] and the transcriptional repressors, Mig1, Mig2 and Nrg1 [68, 73] (involved in glucose repression), regulate the derepression from glucose in *P. pastoris* (Fig. 4B). As in *S. cerevisiae*, these transcription factors are most probably regulated by the SNF1 pathway, as suggested by a high-throughput screen implicating Sak1, the primary Snf1-activating kinase, and Gal83, the  $\beta$ -subunit of the SNF1 complex, in the expression of AOX [74].

In *P. pastoris*, the *S. cerevisiae* transcription activators, Pip2 and Oaf1, have not been found by *in silico* studies. However, methanol and glycerol activate at least two transcription factors, Mit1 and Prm1, which induce enzymes required for methanol utilization (MUT), but not for peroxisome proliferation, by a mechanism resembling Pip2-Oaf1 activation [70, 75].

We analyzed Pex11-2HA, Aox1, Pot1 and Pex3 protein levels under different carbon induction conditions using available kinase deletions strains affecting the SNF1 signaling pathway (Fig. 4C and Fig. 4, figure supplement 1) [74]. As expected, in WT cells, Pex11-2HA, Pot1 and Aox1 were not detected in glucose medium, but glucose derepression (-Glucose) induced Pex11-2HA and Pot1, but not Aox1, which has no role during the growth of WT *P. pastoris* in oleate. Glucose derepression, when combined with the addition of methanol, was needed to observe Aox1 expression in WT cells in our cultivation conditions, indicating a more complex regulation, such as the activation by methanol of Mit1 and Prm1 [70].

We examined Snf1 activation by phosphorylation next because glucose derepression acts via the SNF1 pathway. The amino acid sequence near the activation loop of *P. pastoris* Snf1 (including Thr 171) is identical with that in human AMPK $\alpha$  and *S. cerevisiae* Snf1 [76]. Thus, a phospho-AMPK $\alpha$  (Thr 172) antibody designed to correspond to the residues surrounding Thr 172 of human AMPK $\alpha$  detects the active form of *P. pastoris* Snf1 (Fig. 4, figure supplement 1).

As seen in other organisms, *P. pastoris* Snf1 was activated in WT cells in response to glucose limitation by phosphorylation of Thr 171 of its catalytic subunit (Fig. 4C). A mutant of a putative Tos3 kinase (Tos3<sup>?</sup>; UniProt gene name: PAS\_chr1-3\_0213), with weak homology to its *S. cerevisiae* counterpart, obtained from the *P. pastoris* kinase deletion collection [74], was not required for Snf1 activation, nor for the downstream SNF1 regulation, indicating that PAS\_chr1-3\_0213 is not required for SNF1 signaling or for peroxisomal protein expression. In contrast, Gal83 and Sak1 were essential for Snf1 phosphorylation and the expression of Pex11-2HA, Pot1 and Aox1 in every condition tested, confirming their major role in the SNF1 signaling pathway for the expression of some peroxisomal proteins.

We also analyzed Snf1 activation and expression of the same proteins in the  $\Delta$ nugM strain using the same experimental conditions, and remarkably we observed similar expression defects as those observed for  $\Delta$ sak1 and  $\Delta$ gal83 strains, despite phosphorylation of Snf1 (Fig. 4D). We previously described that DNP causes a similar peroxisome proliferation defect as the OXPHOS mutants (Fig. 3), and like the  $\Delta$ nugM mutant also affects the expression of Pex11, Pot1 and Aox1 during methanol cultivation, despite phosphorylation of Snf1 (Fig. 3, figure supplement 1). Thus, DNP addition phenocopies the OXPHOS mutants in this respect.

We performed quantitative real-time RT-PCR (qRT-PCR) analysis and confirmed that *AOX1*, *PEX11* and *POT1* mRNAs were upregulated in WT in peroxisome proliferation conditions, as expected (Fig. 4E). However, confirming a potential role of OXPHOS in SNF1 signaling,  $\Delta$ nugM cells, like the  $\Delta$ sak1 cells, were unresponsive to oleate and methanol cultivation, and mRNA levels were not significantly upregulated, relative to levels seen in WT cells, in any condition tested.



## **Redox and ATP status of mutants affecting peroxisomal functions**

To confirm our conclusions about the redox and ATP status in mitochondria, peroxisome, NADH shuttles and SNF1 mutants during growth in peroxisome proliferation conditions, we developed cytosolic and peroxisome  $\text{NAD}^+/\text{NADH}$  sensors, and also measured Oxygen Consumption Rate (OCR), which reflects mitochondrial ATP production (Fig. 5). Due to the nature of the assays, we measured  $\text{NAD}^+/\text{NADH}$  ratios in oleate-grown cells and OCR in methanol growing cells. The OCR assay requires the presence of the carbon source in the medium because it measures energy production in live cells in real time and the viscosity of the oleate was incompatible with the instrument. The  $\text{NAD}^+/\text{NADH}$  ratio was measured as an endpoint intensity, so the presence of carbon source was not needed during the assay and was not included during the acquisitions (see Materials and Methods), however the peroxisome sensors are transported to the peroxisomes by the PTS1 pathway, and mislocalization of the sensors will affect the assay. Oleate medium was chosen because the microscopy from Fig. 1 indicated that BFP-PTS1 was transported more efficiently to peroxisomes in oleate medium than in methanol in mutants such as  $\Delta\text{gpdA } \Delta\text{mdhB}$ .

Several fluorescent protein-based  $\text{NAD}^+$  biosensors were recently developed, providing insight into  $\text{NAD}^+$  dynamics. We choose one of these sensors, SoNar, to measure  $\text{NAD}^+/\text{NADH}$  ratios [77]. SoNar was designed using a T-Rex  $\text{NAD}^+$  - and NADH-binding protein linked to cpYFP, and it shows a distinct fluorescence response to NADH and  $\text{NAD}^+$ . That is, the ratio of fluorescence intensities upon excitation at 485 nm and 420 nm decreases in the presence of high concentration of NADH, whereas the ratio increases with higher concentration of  $\text{NAD}^+$ . Like most of these sensors, SoNar is pH sensitive, but this was corrected by measuring SoNar and

cpYFP fluorescence in parallel and normalization of the fluorescence intensity of SoNar with that of cpYFP.

We predicted that during growth in peroxisome proliferation conditions (oleate or methanol), dysfunctional peroxisomes, due to OXPHOS, SNF1, NADH- or acetyl-CoA-shuttling mutants or mutants lacking peroxisomal  $\beta$ -oxidation enzymes, such as Pot1, should not produce peroxisomal NADH, thereby decreasing the cytosolic pool of NADH, which should increase the cytosolic ratio of  $\text{NAD}^+/\text{NADH}$  compared to that in wild-type cells. Indeed, this was confirmed using SoNar (Fig. 5A). Likewise, the ratios of  $\text{NAD}^+/\text{NADH}$  in the peroxisome matrix were also expected to increase for those mutants for the same reasons, except for the NADH-shuttling mutant ( $\Delta\text{gpdA } \Delta\text{mdhB}$ ) which should not increase because NADH cannot shuttle out of the peroxisomes, and this was also corroborated by this assay (Fig. 5A).

In yeast, during growth on non-fermentable carbon sources, most if not all the oxygen, is consumed by OXPHOS to produce ATP. To assess the consequence of our mutants on ATP production during growth in peroxisome proliferation conditions we measured OCR using the Seahorse XF analyzer (Fig. 5B). In addition, the Seahorse analyzer allows measurement of both OCR and the extracellular acidification rate (ECAR) of cells as indicators of glycolysis. The OCR values were significantly reduced in all the mutants tested compared to wild-type, indicating ATP synthesis was seriously impaired. While this was highly expected for OXPHOS mutants, it confirmed the involvement of SNF1, NADH-shuttling, Cat2 and peroxisomal proteins in ATP synthesis during growth in methanol. ECAR, measured for the same samples, showed a significant activity boost after glucose supplementation, a good indication of the cell fitness of the sample set (Fig. 5, figure supplement 1).

**OXPHOS defect in peroxisome proliferation is not rescued by active transcriptional activators of genes encoding peroxisomal proteins**

As Snf1 is phosphorylated in cells with dysfunctional mitochondria, we hypothesized that OXPHOS mutations might affect peroxisomal gene expression downstream of Snf1 activation. We started by analyzing the role of Mit1 (Prm1 was excluded since it acts upstream of Mit1 in the same pathway [70]), which functions during methanol induction and the SNF1-regulated factor, Mxr1, functioning primarily during glucose depression.

Contrary to our expectation that inactivation of one of these transcription factors might mimic the OXPHOS deficiency, we found that none of the deletions,  $\Delta m x r 1$  or  $\Delta m i t 1$ , shared the phenotype of the  $\Delta n u g M$  strain (Fig. 4D and Fig. 6A). During oleate induction, both  $\Delta m x r 1$  and  $\Delta m i t 1$  strains showed only minor defects in Pot1 expression in comparison to WT cells, which was distinct from the behavior of the  $\Delta n u g M$  strain (Fig. 4D). However, during growth in methanol, both transcription activators were essential for Aox1 expression, as described previously [70, 71, 78] (Fig. 6A), confirming again the synergy of signals from the glucose derepression (SNF1 pathway) and from the methanol induction (Prm1 and Mit1) needed to activate the *AOX1* promoter.

The role of these transcription activators was studied further by their direct activation. Briefly, during glucose derepression, the constitutively-expressed Mxr1 is activated by dephosphorylation at Ser 215 [78] and during methanol induction, Prm1 transmits the methanol signal to Mit1 by binding to the *MIT1* promoter, thus increasing expression of Mit1 [70].

We used constitutively-activated transcription activators to bypass any putative deficiencies in their activation in the OXPHOS mutants. We used Mxr1<sup>S215A</sup>, inhibited PKA (PKA mutants are susceptible to 1NM-PP1 inhibition), which is the putative kinase for the

inhibitory phosphorylation of the *S. cerevisiae* homolog of Mxr1 (Adr1), and overexpressed Mit1 (OE-Mit1) from the strong, constitutive *GAPDH* promoter (Fig. 6B and Fig. 6, figure supplement 1).

The plasmids expressing OE-Mit1, PKA mutants and Mxr1<sup>S215A</sup> were transformed into WT,  $\Delta gal83$  and  $\Delta nugM$  strains, respectively, and analyzed for the expression of Pot1 and Aox1 (Fig. 6B and Fig. 6, figure supplement 1). OE-Mit1 reduced the cell fitness independent of the background strain and cells grew slower in all carbon sources tested. Constitutive Mxr1 activation (Mxr1<sup>S215A</sup>) did not affect the fitness of cells, but like OE-Mit1 or PKA inhibition, did not rescue the OXPHOS or SNF1 deficiencies (Fig. 6B and Fig. 6, figure supplement 1).

While Aox1 is strongly induced by methanol, the *AOX1* promoter is strictly repressed by other carbon sources such as glucose, glycerol and ethanol [79]. Recently, the *P. pastoris* MAP kinase, Hog1, was implicated in Aox1 repression under glycerol conditions [74] and in *S. cerevisiae*, Snf1 negatively regulates the activity of Hog1 [80]. However, deletion of the *HOG1* gene in  $\Delta nugM$  cells did not rescue the expression of Pot1 and Aox1 (Fig. 6, figure supplement 1).

### **Rescue of the OXPHOS defect by inactivation of transcriptional repressors of genes encoding peroxisomal proteins**

The regulation of the transcription inhibitors, Mig1, Mig2 and Nrg1 by the SNF1 complex in *S. cerevisiae* has been clearly established, with Snf1 kinase directly phosphorylating Mig1 [37] and Mig2 [40], or directly interacting with Nrg1 [81], causing their release from the promoter of glucose-repressed genes, followed by their export to the cytosol.

In *P. pastoris*, the triple deletion strain ( $\Delta mig1 \Delta mig2 \Delta nrg1$ ) strongly derepressed Aox1 under glycerol-repression conditions, but not during glucose-derepression, even when transcription activators (Mit1 and Prm1) were artificially activated [82]. This makes sense because deletion of *MIG1* and *MIG2* significantly upregulated the binding of Mit1 at the *AOX1* promoter [68].

We used the already available  $\Delta mig1 \Delta mig2 \Delta nrg1$  strain [82], expressing in it Pex3-GFP, and deleted the *NUGM* or *GAL83* (control) genes. Most of the peroxisome proliferation defects we observed in the OXPHOS and *gal83* mutants, such as peroxisome proliferation, as well as Pot1 and Aox1 expression, were rescued when cells were induced in either oleate or methanol (Fig. 7A, B). Both quadruple mutants ( $\Delta mig1 \Delta mig2 \Delta nrg1 \Delta nugM$  and  $\Delta mig1 \Delta mig2 \Delta nrg1 \Delta gal83$ ) behaved similarly in both media. Additionally, peroxisome proliferation was identical to that in WT and the triple mutant ( $\Delta mig1 \Delta mig2 \Delta nrg1$ ) strains (Fig. 7C, D). We observed a reduction in Aox1 expression during oleate induction (glucose derepression) in the  $\Delta mig1 \Delta mig2 \Delta nrg1 \Delta nugM$  strain, in comparison with the WT and the triple mutant strains, but this difference was also observed in  $\Delta mig1 \Delta mig2 \Delta nrg1 \Delta gal83$  strain (Fig. 7A), and was therefore considered insignificant. Thus, most of the peroxisome-associated defects caused the loss of mitochondrial ATP production can be rescued by inactivation of the three transcriptional repressors, closing the mechanistic loop involved in mitochondria-peroxisome interplay.

### **Gal83 nuclear shuttling during peroxisome proliferation is inhibited in OXPHOS mutants**

Transcriptional repressors and activators shuttle between the cytoplasm and the nucleus in a glucose-dependent manner. There is no doubt that the SNF1 complex needs to be localized in the nucleus to inactivate the repressors that occlude the promoters of glucose-repressed genes, but

there is little to no evidence for Mxr1/Adr1 activation in the nucleus. Instead, if Mxr1/Adr1 indeed can be activated within the cytosol, a deficient nuclear enrichment of SNF1 in the OXPHOS mutant during glucose derepression could explain the rescue of peroxisome biogenesis defects in the  $\Delta nugM$  mutant by deletion of the repressors. In *S. cerevisiae*, SNF1 complex localization is regulated by the  $\beta$ -subunits (Gal83, Sip1 and Sip2), with Gal83 being the subunit responsible for the nuclear localization of the complex (referred to hereafter as SNF1-Gal83).

We tested for effects of the of  $\Delta nugM$  mutant on Gal83 nuclear localization by using a Gal83-GFP fusion expressed from the native *GAL83* promoter. WT and mutant cells were grown on abundant glucose, and the nuclear enrichment of Gal83-GFP was stimulated by shifting the cells to oleate for 30 min or methanol for 2 h in the presence leptomycin B (LMB, a potent and specific Crm1 nuclear export inhibitor, required for Gal83 nuclear export in *S. cerevisiae* [83]). As expected, Gal83-GFP was excluded from the nuclei of glucose-grown WT,  $\Delta sak1$  and  $\Delta nugM$  cells (Fig. 8 and Fig. 8, figure supplement 1). Upon the shift to methanol or oleate, Gal83-GFP was enriched in the nucleus of the WT (labelled with the perinuclear ER marker, Sec61-mCherry) and excluded from the nucleus of the  $\Delta sak1$  mutant, as anticipated). Interestingly,  $\Delta nugM$  cells, like  $\Delta sak1$  cells, showed no nuclear enrichment of Gal83-GFP. Together with the Snf1 activation assay (Fig. 4D), these results strongly suggest that the OXPHOS mutants are impaired in the nuclear localization of the SNF1-Gal83 complex independent of the catalytic activation of Snf1 kinase.

#### **Peroxisome proliferation in $\Delta pex14$ cells can be induced by growth in lactate medium**

The aberrant regulation of the SNF1 signaling pathway in cells with dysfunctional mitochondria during glucose derepression, and the lack of a normal peroxisome proliferation in NADH

shuttling mutants during growth in oleate and methanol suggest the presence of a feedback loop between both organelles which goes beyond the initial activation of the SNF1 signaling pathway by glucose derepression. This loop refers to the influence of peroxisomal NADH on mitochondrial ATP production, which in turn feeds back to influence peroxisome biogenesis, division and proliferation.

We tested the feedback loop hypothesis using a strain lacking Pex14, a key member of the peroxisome docking complex and essential for import of peroxisomal matrix proteins [84]. Although normal peroxisomes are absent in cells lacking Pex14, abnormal vesicles containing PMPs but lacking matrix proteins, are observed as peroxisomal remnants. These remnants can be visualized with Pex3-GFP and when we compared  $\Delta pex14$  mutant to WT cells after cultivation in oleate medium, we observed a significantly lower number of peroxisomal structures (Fig. 9). We investigated if an inactive OXPHOS (due to the lack of NADH production by dysfunctional peroxisomes) is the reason for the low number of remnants. We noticed after 4 h of cultivation in L-lactate (lactate) medium (non-fermentable carbon source), that WT cells showed higher levels of Pex11, Aox1 and Pot1 proteins compared to glucose depletion or to cultivation in methanol or oleate (Fig. 4D), which could be a consequence of the lactate metabolism by the mitochondria. Therefore, we used the lactate medium to overcome the low levels of NADH in  $\Delta pex14$  cells, and as we hypothesized, the numbers of peroxisome structures increased in  $\Delta pex14$  cells and were comparable to those in WT cells cultivated in lactate medium.

## Discussion

Organelles are often viewed as individual entities with defined composition and organization that endow them with specialized functions. However, it is now clear that intracellular membrane compartments engage in extensive communication, either indirectly, or directly through membrane contacts [48, 85-88]. Mitochondrial dysfunction impacts several other organelles and their biogenesis, including peroxisomes [89], but the underlying mechanisms have not been elucidated. We have uncovered here the mechanisms involved in one mode of interorganelle communication and interplay in *P. pastoris* where the mitochondria and peroxisomes sense the metabolic status of the cell, influence each other's metabolism, in concert with cytosolic and nuclear involvement, and regulate peroxisome proliferation and division as needed.

## Interorganellar communication and interplay between peroxisomes and mitochondria

In the mitochondrial OXPHOS mutants ( $\Delta$ nugM,  $\Delta$ ndufa9 and  $\Delta$ cyt1), and upon using DNP, peroxisome proliferation, division and biogenesis of several peroxisome-associated proteins, but not peroxisomal matrix protein import (Fig. 2), are affected in cells grown in either methanol or oleate, illustrating the mitochondrial involvement in multiple peroxisomal processes. We extended earlier reports that intermediates of peroxisome metabolism, or the absence of peroxisomal enzymes, regulate the maturation and fission of the organelle [50, 51] by several additional observations. The lack of peroxisomal thiolase (Pot1) affected peroxisome proliferation and division exclusively in oleate. Similarly, the absence of Aox1 and Aox2, involved in the methanol utilization pathway, affected peroxisome proliferation and division only in cells grown in methanol medium (Fig. 1, figure supplement 1). Finally, the lack of Pex5, responsible for the import of PTS1-containing enzymes (including some involved in the  $\beta$ -



oxidation and methanol metabolism pathways), impaired peroxisome proliferation and division in both media (Fig. 1, figure supplement 1). Additionally, blocking the entry of NADH into mitochondria using double deletion strains,  $\Delta mdhA \Delta gpd1$  and  $\Delta mdhB \Delta gpd1$  cells, yielded a phenotype like that seen in the OXPHOS mutants, wherein most of the cells contained only a single, import-competent peroxisome (Fig. 1C). These results are consistent with the role of NADH-shuttling proteins, responsible for shuttling NADH between both peroxisomes and mitochondria via the cytosol (Fig. 5A), in the interorganellar interplay between these organelles, and also points to a role for the cytosol.

#### **Feedback loop between peroxisomes and mitochondria senses cellular metabolic status**

Our results in *P. pastoris* during glucose derepression indicate that peroxisome proliferation, division and biogenesis rely on a functional OXPHOS. Moreover, as methylotrophic yeast rely exclusively on peroxisome metabolism to feed into the mitochondrial OXPHOS for energy production during growth in FA or methanol [90, 91], this feedback loop between the two organelles might contribute to sensing the cell's metabolic status during cultivation in these carbon sources (Fig. 10). Key elements of this feedback loop demonstrated here include the requirement of NADH produced by mitochondria, peroxisomes and NADH shuttles, mitochondrial ATP production, SNF1 activation including Gal83 nuclear translocation and removal of repression by Mig1, Mig2 and Nrg1 for peroxisome biogenesis, division and proliferation. We further validated this feedback loop when we induced the peroxisome proliferation in  $\Delta pex14$  cells, which cannot import peroxisomal matrix proteins or produce NADH, by cultivation in lactate (Fig. 9), which, in yeast, can only be metabolized by mitochondria. Any externally-added lactate will enter mitochondria via a putative lactate/proton symporter and will then be oxidized to pyruvate with a reduction of cytochrome C to generate

ATP [92]. In *Δpex14* cells, cultivation in lactate activated OXPHOS by mitochondrial metabolism and overrode the need for NADH produced by peroxisomal metabolism, boosting peroxisome proliferation (Fig. 9). This also shows clearly that the molecule triggering peroxisome proliferation does not emanate from within peroxisomes, which are dysfunctional in *Δpex14* cells.

### **The OXPHOS effect on peroxisome phenotypes is mediated by the absence of SNF1-Gal83 translocation to the nucleus**

The requirement of ATP we observed for peroxisome biogenesis, division and proliferation is likely mediated through the SNF1 complex that responds to altered cellular AMP/ATP ratios. Our data show that the phenotype of the OXPHOS mutants was due to the inability of the mutants to produce ATP resulting in the lack of nuclear translocation of the SNF1-Gal83 complex (Fig. 8) and a defect in the transcriptional induction of peroxisome division (Pex11) and peroxisomal matrix proteins (e.g. Pot1 and Aox1) in the mutants grown in methanol or oleate (Fig. 4D). This reiterates a nuclear involvement in the activation of peroxisome proliferation.

We present several lines of evidence showing that the newly-discovered role played by OXPHOS in nuclear enrichment of the SNF1-Gal83 complex is separable from its role in catalytic activation of the kinase, and it rather reflects a role in regulating the nuclear relocation of Gal83 itself. First, the *ΔnugM* mutation alone does not affect Thr 210 phosphorylation and activation of Snf1 kinase (Fig. 4D). Second, Gal83 fails to enrich in the nucleus of the *ΔnugM* mutant, under conditions where this relocation is evident in WT cells (Fig. 8). The pathway leading to Gal83 import and the proteins involved in this process are not known. Gal83 may undergo a posttranslational modification upon glucose derepression that could

promote a change in cellular localization. In *S. cerevisiae*, Gal83 phosphorylation sites have been identified in high-throughput studies [93], but the effect of such modifications is not known. Some evidence suggests a role for the mitochondrial voltage-dependent anion channel (VDAC) protein, Por1, promoting Gal83 nuclear localization by a mechanism that is distinct from Snf1 activation during growth in glycerol/ethanol [94], and for the nuclear export receptor, Crm1, in the nuclear exclusion of Gal83 during growth on abundant glucose [83]. *P. pastoris* OXPHOS mutants share phenotypes of  $\Delta Scpor1$  mutant, such as normal Snf1 activation by glucose derepression and the absence of induction of genes regulated by SNF1 signaling [94]. However, the deletion of the only *POR1* homolog, or overexpression of Por1 in *P. pastoris*, did not produce the same phenotypes observed in the OXPHOS mutants and Gal83 localization was unaffected by Por1. Corroborating the role of Gal83 was also the finding the  $\Delta gal83$  cells phenocopied the OXPHOS mutants (Fig. 4C).

#### **The downstream targets of the SNF1-Gal83 signaling explain the peroxisome-related phenotypes in the OXPHOS mutants**

Among the proteins whose expression is affected transcriptionally in the OXPHOS mutants, is Pex11. The Pex11 family of proteins is conserved in yeasts, plants and mammals, and orchestrates peroxisome division [17-19, 95, 96]. Its absence blocks peroxisome division in yeast, but importantly, not its *de novo* proliferation [16], which is seen quite clearly in *P. pastoris* where  $\Delta pex11$  mutants grown in oleate have only 1-2 large peroxisomes, in comparison to WT cells that have about 7 peroxisomes/cell [97]. However, in methanol there is indeed peroxisome proliferation and cells have multiple peroxisomes in cells lacking either Pex11 or its downstream peroxisome division component, Fis1 (unpublished data cited in [97]). Additionally, the *P.*

*pastoris*  $\Delta pex11$  mutant does not phenocopy the OXPHOS mutant (Fig. 11). In both *S. cerevisiae* and *P. pastoris*, Pex11 is induced significantly [25] upon switch from YPD to oleate [97]. In *P. pastoris*, Pex11 is fully repressed upon growth of cells in YPD, whereas in *S. cerevisiae*, Pex11 is expressed at a low level even in YPD [97]. The absence of induction of Pex11 in oleate-grown cells (Fig. 4A, D) is likely the underlying cause for the lack of peroxisome division in the OXPHOS mutants, but would not explain the additional absence of peroxisome proliferation.

The biogenesis defects we observed for peroxisome-associated proteins in the OXPHOS mutants are likely caused by the lack of induction of peroxisomal matrix proteins, such as Pot1 and Aox1 (Fig. 4C-E), and their corresponding RNAs (Fig. 4D). Further corroboration of this conclusion comes from our data that the absence of several peroxisomal matrix proteins (Pot1, Aox1 and Aox2) by deletion of their corresponding genes, or by prevention of their import into peroxisomes (*PEX5* gene deletion) also affects peroxisome proliferation, as seen for the OXPHOS mutants (Fig. 1, figure supplement 1).

Finally, the rescue of the phenotype of the OXPHOS mutant by deletion of the genes encoding the repressors Mig1, Mig2 and Nrg1, extends not only to the induction of *PEX11*, *POT1* and *AOX1* genes (Fig. 7A, B), but also to the reversion of the defect in peroxisome proliferation (Fig. 7C, D), making it very likely that the missing factor required for peroxisome proliferation in the OXPHOS mutants must be a direct or indirect target of these transcriptional repressors, but as argued earlier, based on the peroxisome proliferation seen in  $\Delta pex14$  cells in lactate, this is unlikely to involve a peroxisomal metabolite. In contrast, peroxisome division can be influenced by peroxisomal metabolites [98]. Identification of this proliferation factor remains an important future priority.

We rescued the peroxisome proliferation, peroxisomal protein biogenesis and division defects in the OXPHOS and  $\Delta gal83$  mutants, by the simultaneous deletion of three genes encoding the transcriptional repressors Mig1, Mig2 and Nrg1 (Fig. 7), which repress genes required for peroxisome biogenesis and function [68, 73]. Deletions of the genes for the transcriptional activators, Mit1 and Mxr1, known to activate peroxisome-related genes [70, 71], individually, did not yield the same phenotype as that of the OXPHOS mutants (Fig. 6A), suggesting that these are not directly impaired in the OXPHOS mutants. Additionally, neither overexpression of Mit1, nor artificial activation of Mxr1, rescued the similar phenotypes of the  $\Delta nugM$  and  $\Delta gal83$  mutants (Fig. 6B). Therefore, most of the peroxisome-related phenotypes of the OXPHOS mutants can be explained by the lack of relief of repression of several genes by Mig1, Mig2 and Nrg1, thereby providing a molecular explanation for how the ATP generated by the mitochondria impacts peroxisome proliferation, division and biogenesis.

### **Working model for interorganellar control of peroxisome dynamics**

We present a working model illustrating the interorganellar transactions, communications and signaling that must occur in *P. pastoris* between peroxisomes, cytosol, mitochondria and the nucleus (see Fig. 10 legend for details) for peroxisome proliferation, division and biogenesis of peroxisome-associated proteins. FA uptake and its  $\beta$ -oxidation produce NADH equivalents and acetyl-CoA. However, the peroxisome membrane is impermeable to large hydrophilic solutes, including  $NAD^+$ , NADH,  $NADP^+$  and NADPH, as well as ATP, and either acylated or unacylated coenzyme A (CoA) [54]. Consequently, NADH-shuttling proteins, working together in the peroxisomes, cytosol and mitochondria, allow the delivery of NADH to mitochondria to feed OXPHOS [59]. Acetyl-CoA produced in peroxisomes is delivered to mitochondria via acyl-

carnitine produced in peroxisomes, and mitochondria use the TCA cycle and OXPHOS system for full oxidation to CO<sub>2</sub> and H<sub>2</sub>O [54].

The SNF1/AMP-activated protein kinase (AMPK) complex, which is sensitive to the cellular AMP:ATP ratio, maintains the balance between ATP production and consumption in all eukaryotic cells [65, 66, 76]. Glucose deprivation, which reduces ATP production, activates Snf1 (by phosphorylation) via the action of the Sak1 kinase, and in *P. pastoris*, the nuclear translocation of the SNF1-Gal83 complex requires OXPHOS and ATP production, as shown here. Peroxisome-associated proteins, such as the division protein, Pex11, and the matrix proteins, Pot1 and Aox1, are regulated negatively by transcriptional repressors, that compete with transcriptional activators, such as Mit1 and Mxr1 (equivalent to ScAdr1). Snf1 activation in the cytosol and SNF1-Gal83 entry into the nucleus removes, by phosphorylation of the appropriate proteins, the repression of expression of the peroxisome-associated proteins, while also activating the transcriptional activators. This simultaneous action of SNF1-Gal83 turns on the biogenesis of peroxisome-associated proteins, peroxisome proliferation, as well as division. In the  $\Delta nudM$ ,  $\Delta ndufa9$ ,  $\Delta gal83$ ,  $\Delta pot1$ ,  $\Delta aox1$   $aox2$ , and  $\Delta pex5$  mutants of *P. pastoris*, or in the presence of the mitochondrial uncoupler, DNP, peroxisome proliferation, division and the biogenesis of certain peroxisome-associated proteins is compromised.

In conclusion, since ATP production by mitochondrial OXPHOS is impaired in many human diseases involving over 150 genes [99], including Parkinson's disease and schizophrenia [100-102], as well as during aging [103] and neurodegeneration [104], the results presented here suggest a mechanistic link to peroxisomal dysfunction in human mitochondrial disorders. Further explorations of this yeast model would provide important insights regarding interorganellar communication, interplay and dynamics, while also shedding light on human disease.

585

586

## Materials and Methods

*Methods Availability Statement* - Strains and plasmids are described in Supplementary File 1a (Table S1. Strains and plasmids). Those constructed for the purpose of this study can be requested from the Subramani Lab, following UC San Diego's MTA guidelines (<https://blink.ucsd.edu/research/conducting-research/mta/index.html>).

*Media and reagents used to grow strains* - *P. pastoris* strains were prototrophic without requiring amino acid supplements or yeast extract and were cultivated in minimal media containing different carbon sources. Supplementation of media with amino acids did not change the results of this study. YPD (2% glucose, 2% bacto-peptone, 1% yeast extract), glucose medium (2x YNB [YNB: 0.17% yeast nitrogen base without amino acids and ammonium sulfate, 0.5% ammonium sulfate], 0.04 mg/L biotin, 2% dextrose), oleate medium (2x YNB, 0.04 mg/L biotin, 0.02% Tween-40, 0.2% oleate), and methanol medium (2x YNB, 0.04 mg/L biotin, 1% methanol). Amino acids were supplemented when indicated using 0.79 g/L complete synthetic medium of amino acids and supplements (CSM; #1001, Sunrise Science Products, USA). 2,4-Dinitrophenol (DNP; #D198501, Sigma-Aldrich, USA) was dissolved in methanol, used at a final concentration of 0.25 mM and added after switching cells from glucose to methanol (1%). Leptomycin B solution (LMB; #L2913, Sigma-Aldrich, USA) was added to the methanol medium at final concentration of 200 ng/mL.

*Plasmid constructions* - Plasmids were constructed by Gibson Assembly for which primers were designed using NEBuilder (<https://nebuilder.neb.com/#/>). DNA was amplified from WT genomic DNA by PCR using Advantage 2 Polymerase (#639202, Takara Bio, USA). Plasmid backbones were double-digested with the necessary restriction enzymes and purified using the Qiagen DNA purification kit (#28704X4, QIAGEN GmbH, Germany). DNA inserts were cloned



610 into the digested vectors using the NEBuilder Hifi DNA Assembly Mastermix (#E2621L, New  
611 England Biolabs).

612 *Yeast strain constructions* - Plasmids were linearized with the appropriate restriction enzyme  
613 before transformation of competent yeast cells by electroporation [105]. The transformed cells  
614 were plated on YPD plates with the appropriate selection markers and incubated at 30° C for a  
615 few days. Colonies were screened by Western Blot or fluorescence microscopy.

616 *Fluorescence microscopy* - Cells were grown in YPD at 30° C until exponential phase (1-2  
617 OD<sub>600</sub>/ml), washed twice with sterile water, and then transferred to glucose or peroxisome  
618 proliferation (methanol or oleate) media. With the goal of keeping cells at exponential phase,  
619 different starting OD<sub>600</sub> were used for different strains, depending on the strain's cell doubling  
620 time in the respective media. Cells were grown in indicated media in 250 mL flasks at 30° C and  
621 shaken at 250 rpm. Cells were pelleted, washed twice with sterile water and 1.5µl of cells were  
622 mixed with 1% low melting point agarose and placed on a glass slide with a cover slip and  
623 imaged using 63x or 100× magnification on a Carl Zeiss Axioskop fluorescence microscope.  
624 Images were taken on an AxioCam HR digital camera, no digital gain was used, exposition for  
625 peroxisome markers was kept constant. Images processed on AxioVision software are  
626 representative results from experiments conducted at least in triplicate.

627 *Biochemical studies* - Same conditions described for fluorescence microscopy assays were used  
628 to grow cells. Five OD<sub>600</sub> of cells was collected at different times as described in the figures,  
629 trichloroacetic acid precipitated and analyzed by SDS-PAGE and then by Western blot. The  
630 commercial antibodies used are as follows: Anti-HA (#11666606002, Roche, Germany), Anti-  
631 Snf1 (#100G7E, Cell Signaling Technology, USA) Anti-Rabbit HRP (#172-1019, Bio Rad,  
632 USA), Anti- Mouse HRP (#1706516, Bio Rad, USA), Anti-Rat HRP (#ab97057, Abcam, USA).

633 Additionally, the following antibodies were generated in-house: Anti-Pex2, Anti-Pex3, Anti-  
634 Pot1, Anti-Aox1.

635 *qRT-PCR* - RNA extraction was performed using Trizol™ Reagent (#15596026, Invitrogen,  
636 USA) following the manufacturer's instructions with some modifications. Twenty OD<sub>600</sub> of  
637 frozen cells, grown in the conditions described, were resuspended with 1 mL of Trizol and 250  
638 µl of acid-washed glass beads (425-600 microns). The suspension was vortexed for 30 sec,  
639 followed by chilling on ice for 30 sec. This step was repeated three times. The extraction was  
640 completed according to the protocol described by the kit manufacturer and was followed by  
641 DNase I treatment (#18068015, Life technologies, Carlsbad, CA, USA). The RNA quantity and  
642 quality were determined using the 260/280 nm ratio of approximately 1.8–2.0 for good RNA  
643 quality. The RNA samples were stored at –80° C. cDNA was synthesized from 1 µg of total  
644 RNA using an Invitrogen two-step kit with SuperScript™ III (#18080051, Invitrogen, Carlsbad,  
645 CA, USA) as the reverse transcriptase (RT) enzyme with random hexamer. This was followed by  
646 RNase treatment. The cDNAs were stored at –80° C. One µl of cDNA (equivalent to 80 ng of  
647 total RNA), 300 nM of primers listed in Supplementary File 1b (Table S2. RT-qPCR primers)  
648 and PowerUp™ SYBR™ Green master mix (#A25741, Applied Biosystems, USA) were used.  
649 Values for each target gene were normalized using 18S rRNA and WT in glucose condition as  
650 reference. Expression values were calculated using the  $2^{(-\Delta\Delta CT)}$  method [106].

651 *Metabolic analysis – Biolog Mitoplate assay*: mitochondrial metabolic activity was measured in  
652 digitonin-permeabilized cells using the PM1 MicroPlate (Biolog #12111, Hayward, CA, USA)  
653 following the manufacturer's instructions (protocol document dated February 6, 2019 using cell  
654 preparation protocol Option 1). Briefly, cells were grown in lactate medium, washed and  
655 resuspended in high lactose osmotic stabilizing solution (YMAS), containing digitonin (#D-180-

250, Gold Biotechnology, USA). After 1 h, the permeabilized cells were seeded into 96-well PM1 MicroPlates containing different potential energy substrates. The colorimetric assay was initiated by adding Redox Dye Mix MC (Biolog #74353). The PM1 MicroPlate was then loaded into the OmniLog PM-M system (Biolog, Hayward, CA, USA) for kinetic reading at 30°C. The MitoPlates were read for 24 h at 15 min intervals at OD590. OmniLog rate values were calculated using Data Analysis 1.7 software before being transferred to a Microsoft Excel sheet for reformatting. The software calculates the maximal rate change from the gradient of the reading output during the 24 h time-period. These data are presented as raw OD590 (A.U.).

**Seahorse:** Oxygen consumption rate and extracellular acidification rate were determined in a Seahorse XF96 analyzer. In brief, for the OCR and ECAR analysis, between  $5$  to  $10 \times 10^4$  cells, coming from 15-16 h methanol cultures, were added to a poly-lysine coated Seahorse XF96 PDL Cell Culture Microplate (#103730-100, Agilent, USA) in 50  $\mu$ L of assay medium (XF DMEM medium pH7.4 with 5 mM HEPES without phenol red, sodium bicarbonate, glucose, L-glutamine and sodium pyruvate [#103575, Agilent, USA] supplemented with 6 mM glutamine solution [#103579, Agilent, USA] and 1% methanol). The plate was centrifuged at  $3000 \times g$  for 20 min with gentle acceleration and deceleration. Then 130  $\mu$ L of assay medium were added to each well and incubated at 30°C in a non-CO<sub>2</sub> incubator for 1 h. Immediately following completion of the incubation, OCR and ECAR was measured 3 times every 10 min and an additional 3 times every 30 min after the injection of glucose (2% final concentration; #103577-100, Agilent, USA). All samples were analyzed in triplicate, normalized by cell number and the third stable reading of every condition was plotted in respective graphs.

**SoNar:** NAD<sup>+</sup>/NADH ratio was measured using the genetically encoded sensor, SoNar and its control cpYFP. Cells were pre-grown in oleate medium for 8 h, washed twice and resuspended in

679 2x YNB supplemented with 0.04 mg/L biotin. Between  $2$  to  $3 \times 10^7$  cells in 200  $\mu$ L were seeded  
680 in a 96 well black/clear plate (#353219, BD Falcon, USA) and end point fluorescence intensities  
681 were measured in a NOVOstar Microplate Reader (BMG LABTECH, USA). The SoNar  
682 sensor/cpYFP was excited at 420 nm and 485 nm and the emission at 520 nm was detected to  
683 obtain the ratiometric measurement.  $\text{NAD}^+/\text{NADH}$  ratios were obtained from the emission value  
684 of the 420 nm excitation (F420) and 485 nm excitation (F485). After background subtraction and  
685 normalization for cell number, obtained from absorbance at 600 nm in the same plate reader, the  
686 ratios of  $\text{NAD}^+/\text{NADH}$  were calculated as F420/F480. All samples were analyzed in triplicate.

687   **Acknowledgements**

688   This research was funded by the NIH grant (RO1 DK41737) to SS, who holds a Tata  
689   Chancellor's Endowed Professorship in Molecular Biology. We thank Dr. Barry Bochner and In  
690   Iok Kong from Biolog Inc., Hayward, CA for advice and use of their Biolog machine. We also  
691   thank Agilent for the Seahorse demo unit, Dr. Anthony Molina for access to the Agilent  
692   Seahorse instruments at UCSD and, Dr. Stephan Dozier for advice using the Seahorse analyzer.  
693   Finally, we thank Dr. Y. Yang and Dr. Cai (ECUST, Shanghai, China) for sequences of SoNar  
694   plasmids and *P. pastoris* strains deleted for the transcriptional repressors, respectively, and Dr.  
695   M. Zhou (Shanghai, China) for *P. pastoris* kinase deletion strains.

## Figure legends

Figure 1: **Peroxisome metabolites influence peroxisome size.** (A) Fluorescence microscopy of WT and  $\Delta pot1$  mutant cells expressing Pex3-GFP driven by *PEX3* promoter and BFP-SKL driven by the *GAPDH* promoter, grown in oleate for 8 h. (B) Brief description of FA  $\beta$ -oxidation, methanol metabolism and NADH shuttling between peroxisomes and mitochondria. Cat1, catalase; Cat2: Carnitine acetyl-CoA transferase; Pot1, 3-ketoacylCoA thiolase; Aox, alcohol oxidase; Das, dihydroxyacetone synthase; Fld1, formaldehyde dehydrogenase; Fgh1, S-formylglutathione hydrolase; Fdh1, formate dehydrogenase. (C to F) Fluorescence microscopy of WT, NADH shuttling and  $\Delta cat2$  mutant cells expressing Pex3-GFP and BFP-SKL, grown in oleate for and methanol for 8 h, respectively. Bars: 5  $\mu$ m.

Figure 1, figure supplement 1: **Peroxisome metabolites influence peroxisome size.** (A) Fluorescence microscopy of WT,  $\Delta pot1$  and  $\Delta aox1 \Delta aox2$  cells expressing Pex3-GFP driven and BFP-SKL driven by the *PEX3* the *GAPDH* promoter, respectively. Cells were grown in oleate and methanol for 8 h, respectively. (B) Fluorescence microscopy of WT and  $\Delta pex5$  mutant cells expressing GFP-Pex36 from the *PEX36* promoter. Bars: 5  $\mu$ m

Figure 1, figure supplement 2: **NADH-shuttling mutants influence peroxisome size.** Fluorescence microscopy of WT and NADH-shuttling mutant cells expressing Pex3-GFP and BFP-SKL as in Figure 1, figure supplement 1. Cells were grown in oleate and methanol for 8 h, respectively. Bars: 5  $\mu$ m.

Figure 2: **Dysfunctional mitochondria affect peroxisome proliferation.** (A, B) Fluorescence microscopy of WT, *Δndufa9*, *ΔnugM* and *Δcyt1* mutant cells expressing Pex3-GFP and BFP-SKL, grown for 16 h in (A) oleate and 8 h in (B) methanol medium. Bars: 5  $\mu$ m.

Figure 2, figure supplement 1: **Altered mitochondrial respiration in mitochondrial CI mutants.** Equal amounts of WT, *Δndufa9* and *ΔnugM* cells were grown as described in Materials and Methods, and mitochondrial metabolic activity was measured in digitonin-permeabilized cells using the PM1 MicroPlates from Biolog Inc. Results are presented as the maximum metabolic rates (A.U.). Respiratory substrates are highlighted with boxes. As expected, mitochondrial substrates, producing NADH for CI such as L-lactic acid, citric acid,  $\alpha$ -ketoglutaric acid, pyruvic acid, and others were properly metabolized in WT, but not in the mutant cells. In sharp contrast, CII substrates,  $\alpha$ -glycerol-phosphate, succinic acid and methyl succinate, exhibited unchanged rates of metabolism in the mutants. This result also suggests that CIII activity was not impaired in these CI mutants. Each maximum metabolic rate corresponds to mean  $\pm$  standard deviation (SD) of triplicate values.

Figure 3: **WT cells treated with the OXPHOS uncoupler, DNP, share peroxisome proliferation defects with mitochondrial CI and CIII mutant cells.** Fluorescence microscopy of WT cells expressing Pex3-GFP, grown in methanol medium, with or without 0.25 mM DNP. Bars: 5  $\mu$ m.

Figure 3, figure supplement 1: **Cells treated with the OXPHOS uncoupler, DNP, share same peroxisomal protein expression defects with OXPHOS mutants, without affecting Snf1**

**phosphorylation.** (A) Western blot for several peroxisomal proteins, as well as the total (<sup>T</sup>) the phosphorylated forms (<sup>P</sup>) of Snf1 in cells treated with and without DNP. Specific bands are indicated with an arrow. (B) Ponceau S staining was used as a loading control.

Figure 4: **OXPHOS mutants, like SNF1 mutants impair Pot1, Aox1 and Pex11 expression.**

(A) Western blot of Pex11-2HA visualized with anti-HA antibodies in WT and  $\Delta$ nugM mutant cells. (B) Model of transcriptional regulation of peroxisome genes regulated by SNF1 signaling. ? denotes unknown pathway for induction of Mit1 in oleate. (C) and (D) Western blots of several peroxisomal proteins and the phosphorylated form of Snf1 in WT, SNF1 complex mutants and/or  $\Delta$ nugM mutant cells. Non-specific bands and signal arising from previous western blots are indicated in blue font. Ponceau S staining was used as a loading control. (E) Relative expression of *PEX11*, *POT1* and *AOX1* after 4 h incubation in the indicated carbon source using 18S ribosomal RNA (18S-rRNA) for qPCR normalization, and WT in glucose medium as reference and the  $2^{-\Delta\Delta CT}$  method for the analysis [107].

Figure 4, figure supplement 1: **Peroxisomal protein expression under different environmental conditions and validation of the Phospho-AMPK $\alpha$  (Thr172) antibody in *P.***

*pastoris*. (A) Western blots for several peroxisomal proteins at different time points from wild-type *P. pastoris* cells grown cells in glucose and shifted to no glucose (-glucose), oleate or methanol medium. Ponceau S staining was used as a loading control. (B) Western blots from cell lysates of WT and  $\Delta$ gal83 cells after 30 minutes of methanol induction. The trichloroacetic acid precipitated of both strains, equivalent to 0.5 OD<sub>600</sub>, were loaded in triplicate in a SDS-page gel, transferred to a PVDF membrane and blocked with 5% BSA in TBS with 0.1 % Triton X-100



(TBS-T) for one hour at room temperature. Each triplicated from the PVDF membrane were separated, placed in different boxes containing phosphatase buffer and incubated for 3 hours at 30°C in absence of phosphatase, with 50 units of alkaline phosphatase (CIP; NEB # M0290) or with 1200 units of Lambda protein phosphatase ( $\lambda$  PP; NEB #P0753). After the incubation, the membranes were washed 3 times with TBS-T and incubated with the indicated antibodies. The phosphorylated Snf1 was detected using phospho-AMPK $\alpha$  (Thr172) antibody purchased from Cell Signaling Technology, Inc (#2535). Actin antibody was used as a loading control.

**Figure 5: NAD<sup>+</sup>/NADH ratios and oxygen consumption rates.** (A) NAD<sup>+</sup>/NADH ratios obtained using SoNar sensors from oleate-grown cells [77], as described in Materials and Methods in wild-type and indicated mutant strains. (B) Cell number corrected OCR data from methanol-grown cells for wild-type and mutants from two different parental strains (PPY12h and GS115). Mutants generated from PPY12h:  $\Delta ndufa9$ ,  $\Delta nugM$ ,  $\Delta gpdA$   $\Delta mdhA$ ,  $\Delta aox1$   $\Delta aox2$ ,  $\Delta pex14$  and  $\Delta cat2$ . Mutants generated from GS115:  $\Delta gal83$  and  $\Delta sak1$ . Each point in A and B corresponds to mean  $\pm$  standard deviation (SD) of triplicate values.

**Figure 5, figure supplement 1: Extracellular acidification rates.** ECAR data from methanol and after adding glucose (2% final concentration) for wild-type and mutant cells from two different parental strains (PPY12 or closely related to PPY12, and GS115). Mutants generated from PPY12:  $\Delta ndufa9$ ,  $\Delta nugM$ ,  $\Delta gpdA$   $\Delta mdhA$ ,  $\Delta aox1$   $\Delta aox2$ ,  $\Delta pex14$  and  $\Delta cat2$ . Mutants generated from GS115:  $\Delta gal83$  and  $\Delta sak1$ . Values were normalized using cell numbers and each point corresponds to mean  $\pm$  standard deviation (SD) of triplicate values.

Figure 6: **Analysis of transcriptional activators, Mxr1 and Mit1, of peroxisomal proteins.**

(A) Western blots of Pex3, phospho-Snf1, and Pot1 or Aox1 in WT,  $\Delta mxr1$  and  $\Delta mit1$  mutant cells. (B) Western blots of Pot1 and Aox1 in WT,  $\Delta gal83$  and  $\Delta nugM$  mutant cells, either expressing or not expressing the active form of Mxr1 (Mxr1<sup>S215A</sup>). (C) Western blot of Pot1 in WT,  $\Delta gal83$  and  $\Delta nugM$  mutant cells, without or with overexpression of Mit1 (OE-Mit1). Ponceau S staining was used as a loading control.

Figure 6, figure supplement 1: **PKA inhibition or *HOG1* deletion did not rescue peroxisome proliferation defect of  $\Delta nugM$  mutant cells.** Western blot of Aox1 and Pot1 in WT and  $\Delta nugM$  mutant cells, with and without PKA inhibition or *HOG1* deletion. In *P. pastoris*, PKA consists of a regulatory subunit dimer (Bcy1) and two catalytic subunits (Pka\_A, UniProt gene name: PAS\_chr1-4\_0357; Pka\_B, UniProt gene name: PAS\_chr3\_0964). PKA inhibition was obtained by using a strain with a deletion of PKA\_B gene and a point mutation in Pka\_A (M219G) that renders the kinase sensitive to the drug, 1NM-PP1 (#529606, EMD Millipore, Germany), which was added when cultures were shifted to methanol or oleate medium. Ponceau S staining was used as a loading control.

Figure 7: **Deletion of transcriptional repressors regulated by SNF1 complex signaling rescues  $\Delta nugM$  and  $\Delta gal83$  mutant cells.** (A) and (B) Western blot of Aox1 and Pot1 in WT,  $\Delta nugM$  and  $\Delta gal83$  mutant cells, with and without deletions of genes (*MIG1*, *MIG2* and *NRG1*) encoding the transcriptional repressors regulated by SNF1 signaling. Ponceau S staining was used as a loading control. (C) and (D) Fluorescence microscopy of WT,  $\Delta gal83$  and  $\Delta nugM$  mutant cells expressing Pex3-GFP, with and without deletions of genes (*MIG1*, *MIG2* and

*NRG1*) encoding the transcriptional repressors. Cells were grown in oleate and methanol for 16 h, respectively. Bars: 5  $\mu$ m.

**Figure 8: Gal83 nuclear localization during methanol adaptation is inhibited in  $\Delta$ nugM and  $\Delta$ sak1 mutant cells.** Fluorescence microscopy of WT,  $\Delta$ nugM and  $\Delta$ sak1 mutant cells expressing Gal83-GFP driven by the *GAL83* promoter in presence of 200 ng/mL LMB and Sec71-mCherry as perinuclear ER marker. Bars: 5  $\mu$ m.

**Figure 8, figure supplement 1: Gal83 nuclear localization during oleate adaptation is inhibited in  $\Delta$ nugM mutant cells.** Fluorescence microscopy of WT,  $\Delta$ sak1 and  $\Delta$ nugM mutant cells expressing Gal83-GFP driven by the *GAL83* promoter. Bars: 5  $\mu$ m.

**Figure 9: Cultivation of  $\Delta$ pex14 mutant cells in the respiratory medium, lactate, induces peroxisome proliferation.** Fluorescence microscopy of WT,  $\Delta$ pex14 mutant cells expressing Pex3-GFP in different media for 8 h. Bars: 5  $\mu$ m.

**Figure 10: Interorganellar communication and signaling pathways in peroxisome proliferation, division and matrix protein biogenesis.** Feedback loop between peroxisome and mitochondria is shown in red. FA uptake and its  $\beta$ -oxidation produce NADH equivalents and acetyl-CoA. However, the peroxisome membrane is impermeable to large hydrophilic solutes, including  $\text{NAD}^+$ , NADH,  $\text{NADP}^+$  and NADPH, as well as ATP and acylated or unacylated coenzyme A (CoA) [54]. Consequently, NADH-shuttling proteins, working together in the peroxisomes, cytosol and mitochondria, deliver NADH to mitochondria to feed OXPHOS [59].

Acetyl-CoA produced in peroxisomes is delivered to mitochondria via acyl-carnitine produced in peroxisomes, and mitochondria use the TCA cycle and OXPHOS for full oxidation to CO<sub>2</sub> and H<sub>2</sub>O [54]. The SNF1/AMP-activated protein kinase (AMPK) complex, which is sensitive to the cellular AMP:ATP ratio, maintains the balance between ATP production and consumption [65, 66, 76]. Glucose deprivation, which reduces ATP production, activates Snf1 (by phosphorylation) via the action of the Sak1 kinase, and in *P. pastoris*, the nuclear translocation of the SNF1-Gal83 complex requires OXPHOS and ATP production. Peroxisome-associated proteins, such as the division protein, Pex11, and the matrix proteins, Pot1 and Aox1, are regulated negatively by transcriptional repressors, that compete with transcriptional activators, such as Mit1 and Mxr1 (equivalent to ScAdr1). Snf1 activation in the cytosol and SNF1-Gal83 entry into the nucleus removes, by phosphorylation of the appropriate proteins, the repression of expression of the peroxisome-associated proteins, while also activating the transcriptional activators. This simultaneous action of SNF1-Gal83 turns on the biogenesis of peroxisome-associated proteins, peroxisome proliferation, as well as division. In the  $\Delta nugM$ ,  $\Delta ndufa9$ ,  $\Delta gal83$ ,  $\Delta pot1$ ,  $\Delta aox1$   $\Delta aox2$  and  $\Delta pex5$  mutants of *P. pastoris*, or in the presence of DNP, peroxisome proliferation, division and the biogenesis of certain peroxisome-associated proteins is compromised. FA, fatty acids. PO, peroxisome. P: phosphorylation.

**Figure 11: The  $\Delta pex11$  cells of *P. pastoris* do not phenocopy the OXPHOS mutant, and can proliferate peroxisomes in oleate and methanol.** Peroxisomes are labeled with Pex3-GFP. Bar: 5  $\mu$ m.

## References

1. Sutterlin C, Hsu P, Mallabiabarrena A, Malhotra V (2002) Fragmentation and dispersal of the pericentriolar Golgi complex is required for entry into mitosis in mammalian cells. *Cell* **109**: 359-69
2. Osteryoung KW, Nunnari J (2003) The division of endosymbiotic organelles. *Science* **302**: 1698-704
3. Lingard MJ, Gidda SK, Bingham S, Rothstein SJ, Mullen RT, Trelease RN (2008) *Arabidopsis* PEROXIN11c-e, FISSIN1b, and DYNAMIN-RELATED PROTEIN3A cooperate in cell cycle-associated replication of peroxisomes. *Plant Cell* **20**: 1567-85
4. Hettema EH, Motley AM (2009) How peroxisomes multiply. *J Cell Sci* **122**: 2331-6
5. Guo T, Kit YY, Nicaud JM, Le Dall MT, Sears SK, Vali H, Chan H, Rachubinski RA, Titorenko VI (2003) Peroxisome division in the yeast *Yarrowia lipolytica* is regulated by a signal from inside the peroxisome. *J Cell Biol* **162**: 1255-66
6. Veenhuis M, Kiel JA, Van Der Klei IJ (2003) Peroxisome assembly in yeast. *Microsc Res Tech* **61**: 139-50
7. Farre JC, Subramani S (2016) Mechanistic insights into selective autophagy pathways: lessons from yeast. *Nat Rev Mol Cell Biol* **17**: 537-52
8. Chang CC, South S, Warren D, Jones J, Moser AB, Moser HW, Gould SJ (1999) Metabolic control of peroxisome abundance. *J Cell Sci* **112** ( Pt 10): 1579-90
9. Poll-The BT, Roels F, Ogier H, Scotto J, Vamecq J, Schutgens RB, Wanders RJ, van Roermund CW, van Wijland MJ, Schram AW, *et al.* (1988) A new peroxisomal disorder with enlarged peroxisomes and a specific deficiency of acyl-CoA oxidase (pseudo-neonatal adrenoleukodystrophy). *Am J Hum Genet* **42**: 422-34

- 878 10. Smith JJ, Brown TW, Eitzen GA, Rachubinski RA (2000) Regulation of peroxisome size  
879 and number by fatty acid  $\beta$ -oxidation in the yeast *Yarrowia lipolytica*. *J Biol Chem* **275**: 20168-  
880 78
- 881 11. Yan M, Rayapuram N, Subramani S (2005) The control of peroxisome number and size  
882 during division and proliferation. *Curr Opin Cell Biol* **17**: 376-83
- 883 12. Lazarow PB (2003) Peroxisome biogenesis: advances and conundrums. *Curr Opin Cell*  
884 *Biol* **15**: 489-97
- 885 13. Schrader M (2006) Shared components of mitochondrial and peroxisomal division.  
886 *Biochim Biophys Acta* **1763**: 531-41
- 887 14. Kuravi K, Nagotu S, Krikken AM, Sjollem K, Deckers M, Erdmann R, Veenhuis M,  
888 van der Klei IJ (2006) Dynamin-related proteins Vps1p and Dnm1p control peroxisome  
889 abundance in *Saccharomyces cerevisiae*. *J Cell Sci* **119**: 3994-4001
- 890 15. Motley AM, Ward GP, Hettema EH (2008) Dnm1p-dependent peroxisome fission  
891 requires Caf4p, Mdv1p and Fis1p. *J Cell Sci* **121**: 1633-40
- 892 16. Huber A, Koch J, Kragler F, Brocard C, Hartig A (2012) A subtle interplay between three  
893 Pex11 proteins shapes de novo formation and fission of peroxisomes. *Traffic* **13**: 157-67
- 894 17. Koch J, Brocard C (2012) PEX11 proteins attract Mff and human Fis1 to coordinate  
895 peroxisomal fission. *J Cell Sci* **125**: 3813-26
- 896 18. Koch J, Pranjic K, Huber A, Ellinger A, Hartig A, Kragler F, Brocard C (2010) PEX11  
897 family members are membrane elongation factors that coordinate peroxisome proliferation and  
898 maintenance. *J Cell Sci* **123**: 3389-400
- 899 19. Aung K, Zhang X, Hu J (2010) Peroxisome division and proliferation in plants. *Biochem*  
900 *Soc Trans* **38**: 817-22

- 901 20. Thoms S, Gartner J (2012) First PEX11 $\beta$  patient extends spectrum of peroxisomal  
902 biogenesis disorder phenotypes. *J Med Genet* **49**: 314-6
- 903 21. Wang J, Li L, Zhang Z, Qiu H, Li D, Fang Y, Jiang H, Chai RY, Mao X, Wang Y, *et al.*  
904 (2015) One of three Pex11 family members is required for peroxisomal proliferation and full  
905 virulence of the rice blast fungus *Magnaporthe oryzae*. *PLoS One* **10**: e0134249
- 906 22. Weng H, Ji X, Naito Y, Endo K, Ma X, Takahashi R, Shen C, Hirokawa G, Fukushima  
907 Y, Iwai N (2013) Pex11 $\alpha$  deficiency impairs peroxisome elongation and division and contributes  
908 to nonalcoholic fatty liver in mice. *Am J Physiol Endocrinol Metab* **304**: E187-96
- 909 23. Gurvitz A, Rottensteiner H (2006) The biochemistry of oleate induction: transcriptional  
910 upregulation and peroxisome proliferation. *Biochim Biophys Acta* **1763**: 1392-402
- 911 24. Scheckhuber CQ (2019) Characterization of survival and stress resistance in *S. cerevisiae*  
912 mutants affected in peroxisome inheritance and proliferation,  $\Delta inp1$  and  $\Delta pex11$ . *Folia Microbiol*  
913 (*Praha*) 2020 Apr;65(2):423-429. doi: 10.1007/s12223-019-00724-0.
- 914 25. Karpichev IV, Small GM (1998) Global regulatory functions of Oaf1p and Pip2p  
915 (Oaf2p), transcription factors that regulate genes encoding peroxisomal proteins in  
916 *Saccharomyces cerevisiae*. *Mol Cell Biol* **18**: 6560-70
- 917 26. Smith JJ, Marelli M, Christmas RH, Vizeacoumar FJ, Dilworth DJ, Ideker T, Galitski T,  
918 Dimitrov K, Rachubinski RA, Aitchison JD (2002) Transcriptome profiling to identify genes  
919 involved in peroxisome assembly and function. *J Cell Biol* **158**: 259-71
- 920 27. Rottensteiner H, Kal AJ, Filipits M, Binder M, Hamilton B, Tabak HF, Ruis H (1996)  
921 Pip2p: a transcriptional regulator of peroxisome proliferation in the yeast *Saccharomyces*  
922 *cerevisiae*. *EMBO J* **15**: 2924-34

- 923 28. Rottensteiner H, Wabnegger L, Erdmann R, Hamilton B, Ruis H, Hartig A, Gurvitz A  
924 (2003) *Saccharomyces cerevisiae* PIP2 mediating oleic acid induction and peroxisome  
925 proliferation is regulated by Adr1p and Pip2p-Oaf1p. *J Biol Chem* **278**: 27605-11
- 926 29. Jiang R, Carlson M (1997) The Snf1 protein kinase and its activating subunit, Snf4,  
927 interact with distinct domains of the Sip1/Sip2/Gal83 component in the kinase complex. *Mol*  
928 *Cell Biol* **17**: 2099-106
- 929 30. Yang X, Jiang R, Carlson M (1994) A family of proteins containing a conserved domain  
930 that mediates interaction with the yeast SNF1 protein kinase complex. *EMBO J* **13**: 5878-86
- 931 31. Vincent O, Townley R, Kuchin S, Carlson M (2001) Subcellular localization of the Snf1  
932 kinase is regulated by specific beta subunits and a novel glucose signaling mechanism. *Genes*  
933 *Dev* **15**: 1104-14
- 934 32. Elbing K, McCartney RR, Schmidt MC (2006) Purification and characterization of the  
935 three Snf1-activating kinases of *Saccharomyces cerevisiae*. *Biochem J* **393**: 797-805
- 936 33. Hedbacker K, Hong SP, Carlson M (2004) Pak1 protein kinase regulates activation and  
937 nuclear localization of Snf1-Gal83 protein kinase. *Mol Cell Biol* **24**: 8255-63
- 938 34. Hong SP, Leiper FC, Woods A, Carling D, Carlson M (2003) Activation of yeast Snf1  
939 and mammalian AMP-activated protein kinase by upstream kinases. *Proc Natl Acad Sci U S A*  
940 **100**: 8839-43
- 941 35. Vallier LG, Carlson M (1994) Synergistic release from glucose repression by *mig1* and  
942 *ssn* mutations in *Saccharomyces cerevisiae*. *Genetics* **137**: 49-54
- 943 36. Serra-Cardona A, Petrezselyova S, Canadell D, Ramos J, Arino J (2014) Coregulated  
944 expression of the Na<sup>+</sup>/phosphate Pho89 transporter and Ena1 Na<sup>+</sup>-ATPase allows their functional  
945 coupling under high-pH stress. *Mol Cell Biol* **34**: 4420-35



- 946 37. Treitel MA, Kuchin S, Carlson M (1998) Snf1 protein kinase regulates phosphorylation  
947 of the Mig1 repressor in *Saccharomyces cerevisiae*. *Mol Cell Biol* **18**: 6273-80
- 948 38. Young ET, Dombek KM, Tachibana C, Ideker T (2003) Multiple pathways are co-  
949 regulated by the protein kinase Snf1 and the transcription factors Adr1 and Cat8. *J Biol Chem*  
950 **278**: 26146-58
- 951 39. Prielhofer R, Cartwright SP, Graf AB, Valli M, Bill RM, Mattanovich D, Gasser B  
952 (2015) *Pichia pastoris* regulates its gene-specific response to different carbon sources at the  
953 transcriptional, rather than the translational, level. *BMC Genomics* **16**: 167
- 954 40. Chandrashekarappa DG, McCartney RR, Schmidt MC (2011) Subunit and domain  
955 requirements for adenylate-mediated protection of Snf1 kinase activation loop from  
956 dephosphorylation. *J Biol Chem* **286**: 44532-41
- 957 41. Ludin K, Jiang R, Carlson M (1998) Glucose-regulated interaction of a regulatory subunit  
958 of protein phosphatase 1 with the Snf1 protein kinase in *Saccharomyces cerevisiae*. *Proc Natl*  
959 *Acad Sci U S A* **95**: 6245-50
- 960 42. Mayer FV, Heath R, Underwood E, Sanders MJ, Carmena D, McCartney RR, Leiper FC,  
961 Xiao B, Jing C, Walker PA, *et al.* (2011) ADP regulates SNF1, the *Saccharomyces cerevisiae*  
962 homolog of AMP-activated protein kinase. *Cell Metab* **14**: 707-14
- 963 43. Dakik P, Titorenko VI (2016) Communications between mitochondria, the nucleus,  
964 vacuoles, peroxisomes, the endoplasmic reticulum, the plasma membrane, lipid droplets, and the  
965 cytosol during yeast chronological aging. *Front Genet* **7**: 177
- 966 44. Mattiazzi Usaj M, Brloznik M, Kaferle P, Zitnik M, Wolinski H, Leitner F, Kohlwein  
967 SD, Zupan B, Petrovic U (2015) Genome-wide localization study of yeast Pex11 identifies  
968 peroxisome-mitochondria interactions through the ERMES complex. *J Mol Biol* **427**: 2072-87

- 969 45. Shai N, Yifrach E, van Roermund CWT, Cohen N, Bibi C, L IJ, Cavellini L, Meurisse J,  
970 Schuster R, Zada L, *et al.* (2018) Systematic mapping of contact sites reveals tethers and a  
971 function for the peroxisome-mitochondria contact. *Nat Commun* **9**: 1761, doi: 10.1038/s41467-  
972 018-03957-8
- 973 46. Baumgart E, Vanhorebeek I, Grabenbauer M, Borgers M, Declercq PE, Fahimi HD, Baes  
974 M (2001) Mitochondrial alterations caused by defective peroxisomal biogenesis in a mouse  
975 model for Zellweger syndrome (PEX5 knockout mouse). *Am J Pathol* **159**: 1477-94
- 976 47. Salpietro V, Phadke R, Saggar A, Hargreaves IP, Yates R, Fokoloros C, Mankad K,  
977 Hertecant J, Ruggieri M, McCormick D, *et al.* (2015) Zellweger syndrome and secondary  
978 mitochondrial myopathy. *Eur J Pediatr* **174**: 557-63
- 979 48. Fransen M, Lismont C, Walton P (2017) The peroxisome-mitochondria connection: how  
980 and why? *Int J Mol Sci* **18**: 1126, doi: 10.3390/ijms18061126
- 981 49. Gould SJ, McCollum D, Spong AP, Heyman JA, Subramani S (1992) Development of  
982 the yeast *Pichia pastoris* as a model organism for a genetic and molecular analysis of  
983 peroxisome assembly. *Yeast* **8**: 613-28
- 984 50. Nguyen T, Bjorkman J, Paton BC, Crane DI (2006) Failure of microtubule-mediated  
985 peroxisome division and trafficking in disorders with reduced peroxisome abundance. *J Cell Sci*  
986 **119**: 636-45
- 987 51. Espeel M, Depreter M, Nardacci R, D'Herde K, Kerckaert I, Stefanini S, Roels F (1997)  
988 Biogenesis of peroxisomes in fetal liver. *Microsc Res Tech* **39**: 453-66
- 989 52. Mahalingam SS, Shukla N, Farre JC, Zientara-Rytter K, Subramani S (2021) Balancing  
990 the opposing principles that govern peroxisome homeostasis. *Trends Biochem Sci* **46**: 200-212

991 53. Reinisch KM, Prinz WA (2021) Mechanisms of nonvesicular lipid transport. *J Cell Biol*  
992 **220**: e202012058. doi: 10.1083/jcb.202012058

993 54. Wanders RJA, Vaz FM, Waterham HR, Ferdinandusse S (2020) Fatty acid oxidation in  
994 peroxisomes: enzymology, metabolic crosstalk with other organelles and peroxisomal disorders.  
995 *Adv Exp Med Biol* **1299**: 55-70

996 55. Al-Saryi NA, Al-Hejjaj MY, van Roermund CWT, Hulmes GE, Ekal L, Payton C,  
997 Wanders RJA, Hettema EH (2017) Two NAD-linked redox shuttles maintain the peroxisomal  
998 redox balance in *Saccharomyces cerevisiae*. *Sci Rep* **7**: 11868, doi: 10.1038/s41598-017-11942-2

999 56. Gabay-Maskit S, Cruz-Zaragoza LD, Shai N, Eisenstein M, Bibi C, Cohen N, Hansen T,  
1000 Yifrach E, Harpaz N, Belostotsky R, *et al.* (2020) A piggybacking mechanism enables  
1001 peroxisomal localization of the glyoxylate cycle enzyme Mdh2 in yeast. *J Cell Sci* **133**:  
1002 jcs244376, doi: 10.1242/jcs.244376

1003 57. Kumar S, Singh R, Williams CP, van der Klei IJ (2016) Stress exposure results in  
1004 increased peroxisomal levels of yeast Pnc1 and Gpd1, which are imported via a piggy-backing  
1005 mechanism. *Biochim Biophys Acta* **1863**: 148-56

1006 58. Ansell R, Granath K, Hohmann S, Thevelein JM, Adler L (1997) The two isoenzymes for  
1007 yeast NAD<sup>+</sup>-dependent glycerol 3-phosphate dehydrogenase encoded by *GPD1* and *GPD2* have  
1008 distinct roles in osmoadaptation and redox regulation. *EMBO J* **16**: 2179-87

1009 59. Farre JC, Li P, Subramani S (2021) BiFC method based on intraorganellar protein  
1010 crowding detects oleate-dependent peroxisomal targeting of *Pichia pastoris* malate  
1011 dehydrogenase. *Int J Mol Sci* **22**: 4890, doi: 10.3390/ijms22094890

- 1012 60. van Roermund CW, Elgersma Y, Singh N, Wanders RJ, Tabak HF (1995) The membrane  
1013 of peroxisomes in *Saccharomyces cerevisiae* is impermeable to NAD(H) and acetyl-CoA under  
1014 in vivo conditions. *EMBO J* **14**: 3480-6
- 1015 61. Camara E, Landes N, Albiol J, Gasser B, Mattanovich D, Ferrer P (2017) Increased  
1016 dosage of AOX1 promoter-regulated expression cassettes leads to transcription attenuation of the  
1017 methanol metabolism in *Pichia pastoris*. *Sci Rep* **7**: 44302. doi: 10.1038/srep44302
- 1018 62. Lasserre JP, Dautant A, Aiyar RS, Kucharczyk R, Glatigny A, Tribouillard-Tanvier D,  
1019 Rytka J, Blondel M, Skoczen N, Reynier P, *et al.* (2015) Yeast as a system for modeling  
1020 mitochondrial disease mechanisms and discovering therapies. *Dis Model Mech* **8**: 509-26
- 1021 63. Pinchot GB (1967) The mechanism of uncoupling of oxidative phosphorylation by 2,4-  
1022 dinitrophenol. *J Biol Chem* **242**: 4577-83
- 1023 64. Hedbacker K, Carlson M (2008) SNF1/AMPK pathways in yeast. *Front Biosci* **13**: 2408-  
1024 20
- 1025 65. Kayikci O, Nielsen J (2015) Glucose repression in *Saccharomyces cerevisiae*. *FEMS*  
1026 *Yeast Res* **15**: fov068. doi: 10.1093/femsyr/fov068
- 1027 66. Kim JH, Roy A, Jouandot D, 2nd, Cho KH (2013) The glucose signaling network in  
1028 yeast. *Biochim Biophys Acta* **1830**: 5204-10
- 1029 67. Saleem RA, Knoblauch B, Mast FD, Smith JJ, Boyle J, Dobson CM, Long-O'Donnell R,  
1030 Rachubinski RA, Aitchison JD (2008) Genome-wide analysis of signaling networks regulating  
1031 fatty acid-induced gene expression and organelle biogenesis. *J Cell Biol* **181**: 281-92
- 1032 68. Shi L, Wang X, Wang J, Zhang P, Qi F, Cai M, Zhang Y, Zhou X (2018) Transcriptome  
1033 analysis of  $\Delta mig1 \Delta mig2$  mutant reveals their roles in methanol catabolism, peroxisome  
1034 biogenesis and autophagy in methylotrophic yeast *Pichia pastoris*. *Genes Genomics* **40**: 399-412

- 1035 69. Vogl T, Sturmberger L, Fauland PC, Hyden P, Fischer JE, Schmid C, Thallinger GG,  
1036 Geier M, Glieder A (2018) Methanol independent induction in *Pichia pastoris* by simple  
1037 derepressed overexpression of single transcription factors. *Biotechnol Bioeng* **115**: 1037-1050
- 1038 70. Wang X, Wang Q, Wang J, Bai P, Shi L, Shen W, Zhou M, Zhou X, Zhang Y, Cai M  
1039 (2016) Mit1 transcription factor mediates methanol signaling and regulates the alcohol oxidase 1  
1040 (AOX1) promoter in *Pichia pastoris*. *J Biol Chem* **291**: 6245-61
- 1041 71. Lin-Cereghino GP, Godfrey L, de la Cruz BJ, Johnson S, Khuongsathiene S, Tolstorukov  
1042 I, Yan M, Lin-Cereghino J, Veenhuis M, Subramani S, *et al.* (2006) Mxr1p, a key regulator of  
1043 the methanol utilization pathway and peroxisomal genes in *Pichia pastoris*. *Mol Cell Biol* **26**:  
1044 883-97
- 1045 72. Hou C, Yang Y, Xing Y, Zhan C, Liu G, Liu X, Liu C, Zhan J, Xu D, Bai Z (2020)  
1046 Targeted editing of transcriptional activator MXR1 on the *Pichia pastoris* genome using  
1047 CRISPR/Cas9 technology. *Yeast* **37**: 305-312
- 1048 73. Wang X, Cai M, Shi L, Wang Q, Zhu J, Wang J, Zhou M, Zhou X, Zhang Y (2016)  
1049 PpNrg1 is a transcriptional repressor for glucose and glycerol repression of AOX1 promoter in  
1050 methylotrophic yeast *Pichia pastoris*. *Biotechnol Lett* **38**: 291-8
- 1051 74. Shen W, Kong C, Xue Y, Liu Y, Cai M, Zhang Y, Jiang T, Zhou X, Zhou M (2016)  
1052 Kinase screening in *Pichia pastoris* identified promising targets involved in cell growth and  
1053 alcohol oxidase 1 promoter (P<sub>AOX1</sub>) regulation. *PLoS One* **11**: e0167766
- 1054 75. Sahu U, Krishna Rao K, Rangarajan PN (2014) Trm1p, a Zn(II)(2)Cys(6)-type  
1055 transcription factor, is essential for the transcriptional activation of genes of methanol utilization  
1056 pathway, in *Pichia pastoris*. *Biochem Biophys Res Commun* **451**: 158-64

- 1057 76. Yan Y, Zhou XE, Xu HE, Melcher K (2018) Structure and physiological regulation of  
1058 AMPK. *Int J Mol Sci* **19**
- 1059 77. Zhao Y, Hu Q, Cheng F, Su N, Wang A, Zou Y, Hu H, Chen X, Zhou HM, Huang X, *et*  
1060 *al.* (2015) SoNar, a highly responsive NAD<sup>+</sup>/NADH sensor, allows high-throughput metabolic  
1061 screening of anti-tumor agents. *Cell Metab* **21**: 777-89
- 1062 78. Parua PK, Ryan PM, Trang K, Young ET (2012) *Pichia pastoris* 14-3-3 regulates  
1063 transcriptional activity of the methanol inducible transcription factor Mxr1 by direct interaction.  
1064 *Mol Microbiol* **85**: 282-98
- 1065 79. Hartner FS, Glieder A (2006) Regulation of methanol utilisation pathway genes in yeasts.  
1066 *Microb Cell Fact* **5**: 39, doi: 10.1186/1475-2859-5-39
- 1067 80. Mizuno T, Masuda Y, Irie K (2015) The *Saccharomyces cerevisiae* AMPK, Snf1,  
1068 negatively regulates the Hog1 MAPK pathway in ER stress response. *PLoS Genet* **11**: e1005491,  
1069 doi: 10.1371/journal.pgen.1005491
- 1070 81. Vyas VK, Kuchin S, Carlson M (2001) Interaction of the repressors Nrg1 and Nrg2 with  
1071 the Snf1 protein kinase in *Saccharomyces cerevisiae*. *Genetics* **158**: 563-72
- 1072 82. Wang J, Wang X, Shi L, Qi F, Zhang P, Zhang Y, Zhou X, Song Z, Cai M (2017)  
1073 Methanol-independent protein expression by *AOX1* promoter with trans-acting elements  
1074 engineering and glucose-glycerol-shift induction in *Pichia pastoris*. *Sci Rep* **7**: 41850, doi:  
1075 10.1038/srep41850
- 1076 83. Hedbacker K, Carlson M (2006) Regulation of the nucleocytoplasmic distribution of  
1077 Snf1-Gal83 protein kinase. *Eukaryot Cell* **5**: 1950-6
- 1078 84. Farre JC, Mahalingam SS, Proietto M, Subramani S (2019) Peroxisome biogenesis,  
1079 membrane contact sites, and quality control. *EMBO Rep* **20**: e46864.

doi: 10.15252/embr.201846864

85. Castro IG, Schuldiner M, Zalckvar E (2018) Mind the organelle gap - peroxisome contact sites in disease. *Trends Biochem Sci* **43**: 199-210

86. Chu BB, Liao YC, Qi W, Xie C, Du X, Wang J, Yang H, Miao HH, Li BL, Song BL (2015) Cholesterol transport through lysosome-peroxisome membrane contacts. *Cell* **161**: 291-306

87. Schuldiner M, Zalckvar E (2017) Incredibly close-A newly identified peroxisome-ER contact site in humans. *J Cell Biol* **216**: 287-289

88. Shai N, Schuldiner M, Zalckvar E (2016) No peroxisome is an island - peroxisome contact sites. *Biochim Biophys Acta* **1863**: 1061-9

89. Diogo CV, Yambire KF, Fernandez Mosquera L, Branco FT, Raimundo N (2018) Mitochondrial adventures at the organelle society. *Biochem Biophys Res Commun* **500**: 87-93

90. Kurihara T, Ueda M, Okada H, Kamasawa N, Naito N, Osumi M, Tanaka A (1992) Beta-oxidation of butyrate, the short-chain-length fatty acid, occurs in peroxisomes in the yeast *Candida tropicalis*. *J Biochem* **111**: 783-7

91. Tanaka A, Osumi M, Fukui S (1982) Peroxisomes of alkane-grown yeast: fundamental and practical aspects. *Ann N Y Acad Sci* **386**: 183-99

92. Passarella S, de Bari L, Valenti D, Pizzuto R, Paventi G, Atlante A (2008) Mitochondria and L-lactate metabolism. *FEBS Lett* **582**: 3569-76

93. Lanz MC, Yugandhar K, Gupta S, Sanford EJ, Faca VM, Vega S, Joiner AMN, Fromme JC, Yu H, Smolka MB (2021) In-depth and 3-dimensional exploration of the budding yeast phosphoproteome. *EMBO Rep* **22**: e51121. doi: 10.15252/embr.202051121

1102 94. Shevade A, Strogolova V, Orlova M, Yeo CT, Kuchin S (2018) Mitochondrial voltage-  
1103 dependent anion channel protein Por1 positively regulates the nuclear localization of  
1104 *Saccharomyces cerevisiae* AMP-activated protein kinase. *mSphere* 3(1):e00482-17. doi:  
1105 10.1128/mSphere.00482-17.

1106 95. Tam YY, Torres-Guzman JC, Vizeacoumar FJ, Smith JJ, Marelli M, Aitchison JD,  
1107 Rachubinski RA (2003) Pex11-related proteins in peroxisome dynamics: a role for the novel  
1108 peroxin Pex27p in controlling peroxisome size and number in *Saccharomyces cerevisiae*. *Mol*  
1109 *Biol Cell* **14**: 4089-102

1110 96. Thoms S, Erdmann R (2005) Dynamin-related proteins and Pex11 proteins in peroxisome  
1111 division and proliferation. *FEBS J* **272**: 5169-81

1112 97. Joshi S, Agrawal G, Subramani S (2012) Phosphorylation-dependent Pex11p and Fis1p  
1113 interaction regulates peroxisome division. *Mol Biol Cell* **23**: 1307-15

1114 98. Rinaldi MA, Patel AB, Park J, Lee K, Strader LC, Bartel B (2016) The roles of  $\beta$ -  
1115 oxidation and cofactor homeostasis in peroxisome distribution and function in *Arabidopsis*  
1116 *thaliana*. *Genetics* **204**: 1089-1115

1117 99. Liu S, Liu S, He B, Li L, Li L, Wang J, Cai T, Chen S, Jiang H (2021) OXPHOS  
1118 deficiency activates global adaptation pathways to maintain mitochondrial membrane potential.  
1119 *EMBO Rep* **22**: e51606, doi: 10.15252/embr.202051606

1120 100. Bergman O, Ben-Shachar D (2016) Mitochondrial oxidative phosphorylation system  
1121 (OXPHOS) deficits in schizophrenia: possible interactions with cellular processes. *Can J*  
1122 *Psychiatry* **61**: 457-69

1123 101. Lopez-Gallardo E, Iceta R, Iglesias E, Montoya J, Ruiz-Pesini E (2011) OXPHOS  
1124 toxicogenomics and Parkinson's disease. *Mutat Res* **728**: 98-106



1125 102. Zhu Z, Wang X (2017) Significance of mitochondria DNA mutations in diseases. *Adv*  
1126 *Exp Med Biol* **1038**: 219-230

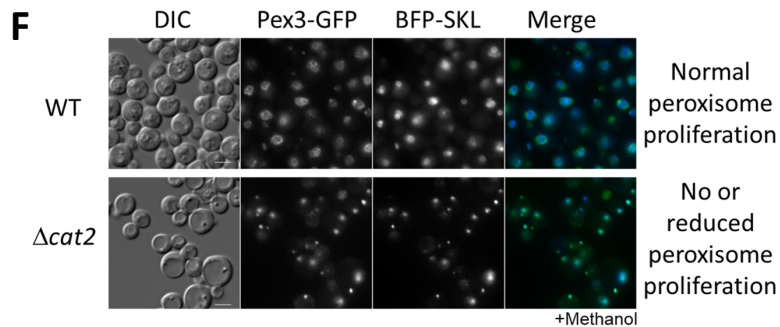
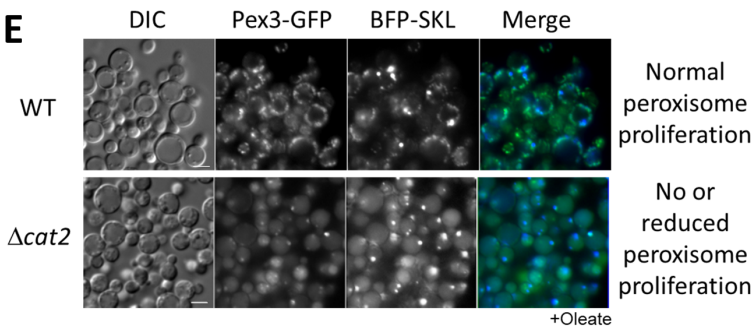
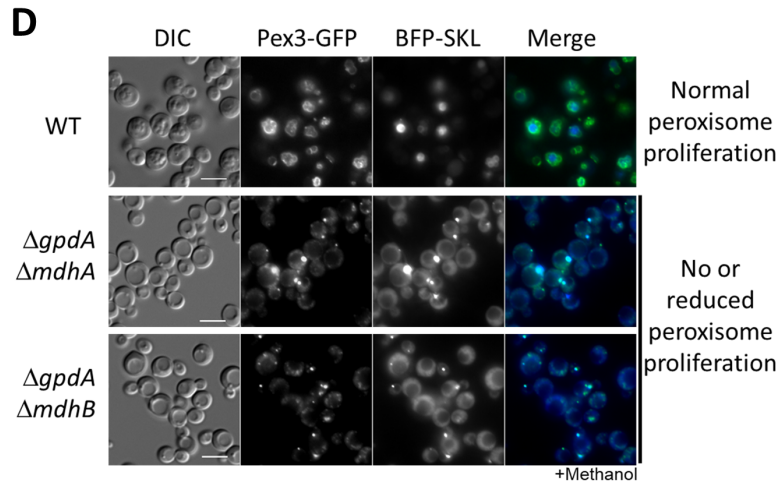
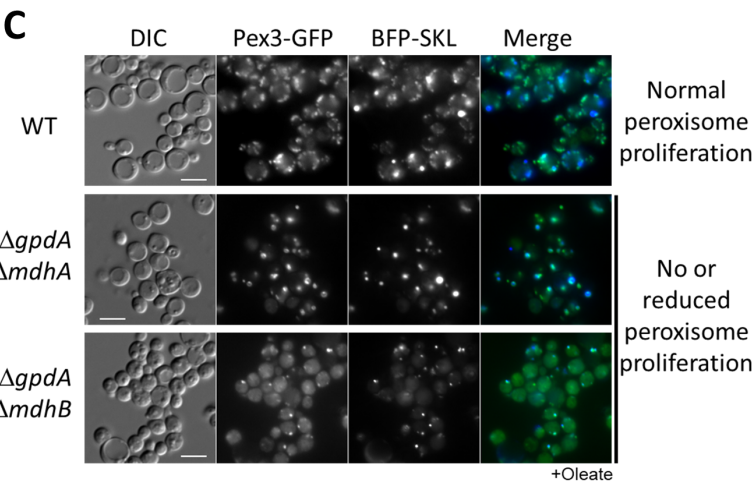
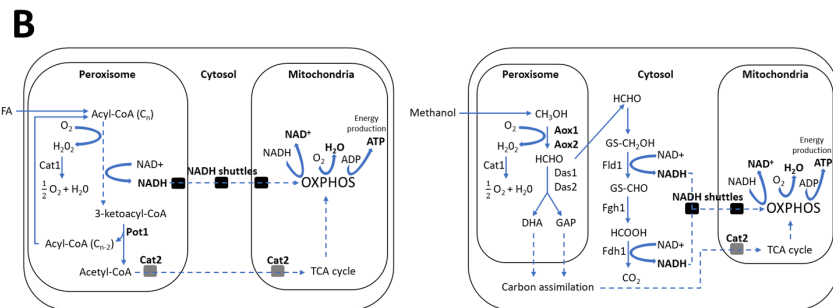
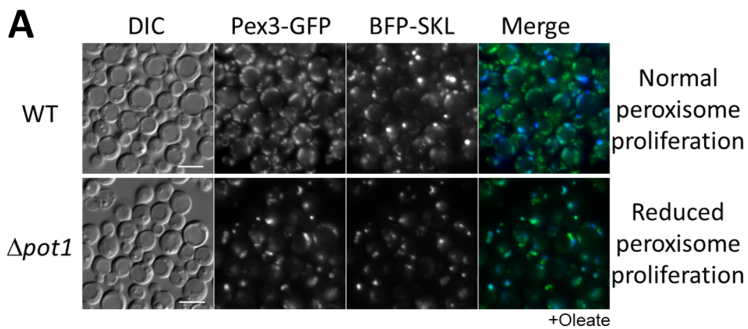
1127 103. Olgun A, Akman S (2007) Mitochondrial DNA-deficient models and aging. *Ann N Y*  
1128 *Acad Sci* **1100**: 241-5

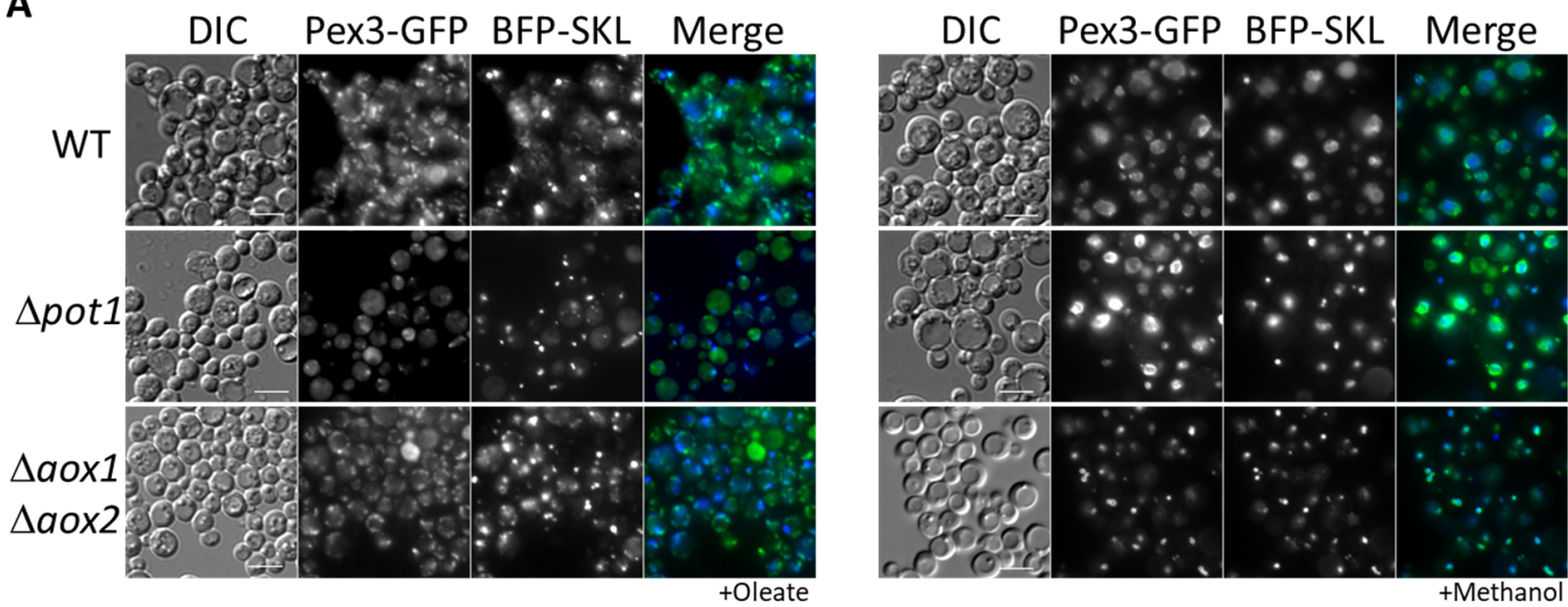
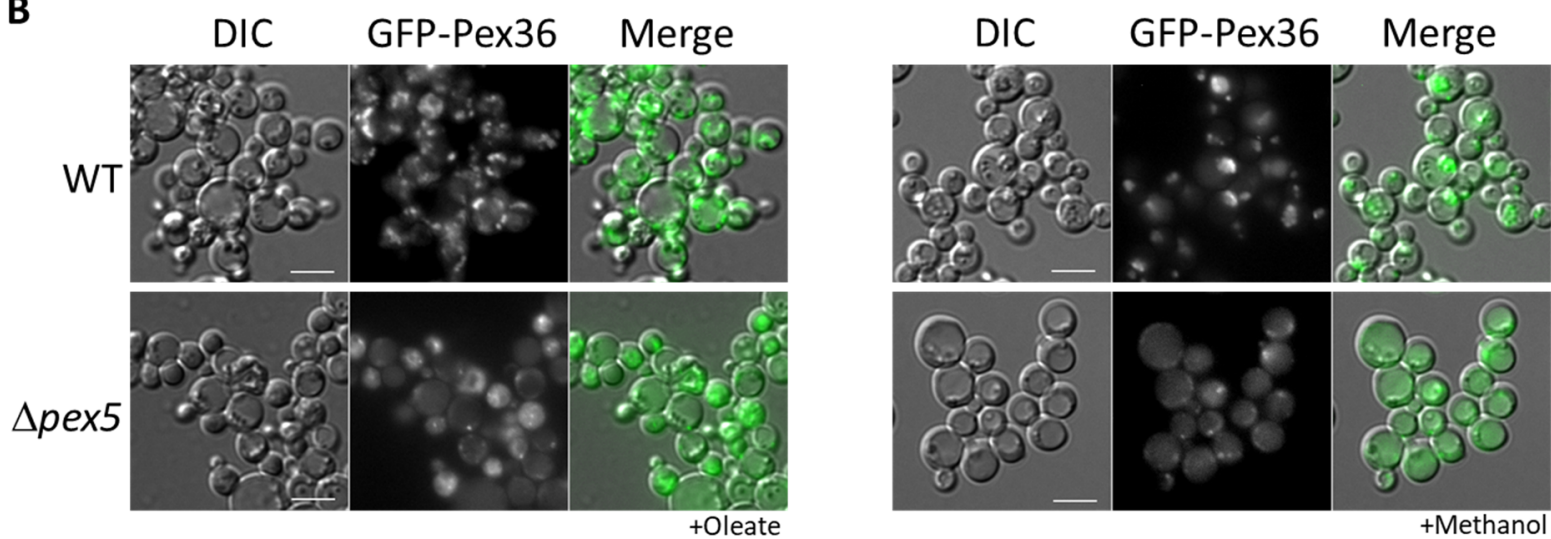
1129 104. Koopman WJ, Distelmaier F, Smeitink JA, Willems PH (2013) OXPHOS mutations and  
1130 neurodegeneration. *EMBO J* **32**: 9-29

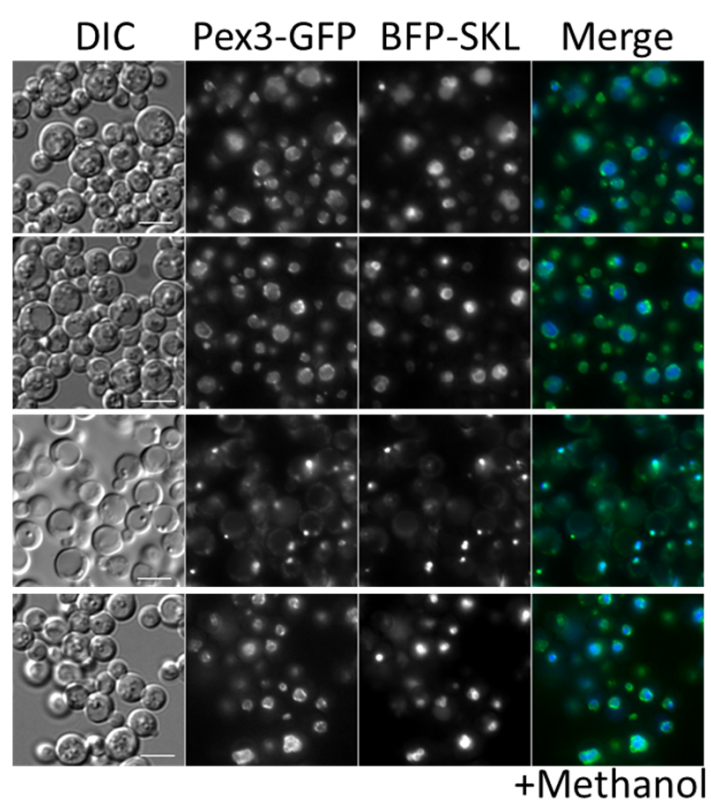
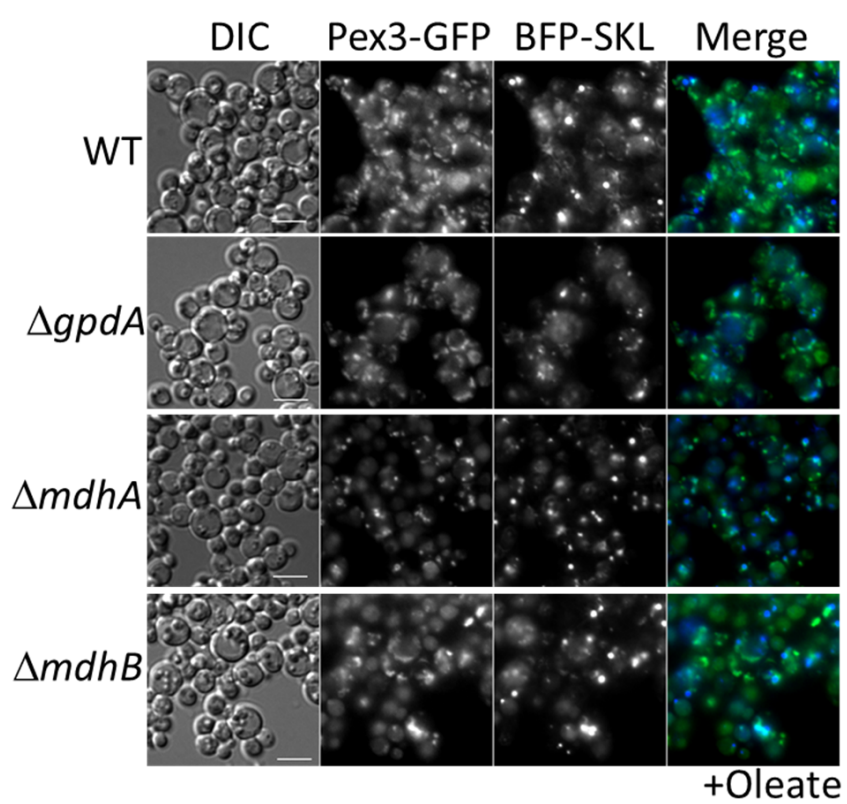
1131 105. Cregg JM, Russell KA (1998) Transformation. *Methods Mol Biol* **103**: 27-39

1132 106. Livak KJ, Schmittgen TD (2001) Analysis of relative gene expression data using real-  
1133 time quantitative PCR and the  $2^{(-\Delta\Delta CT)}$  method. *Methods* **25**: 402-8

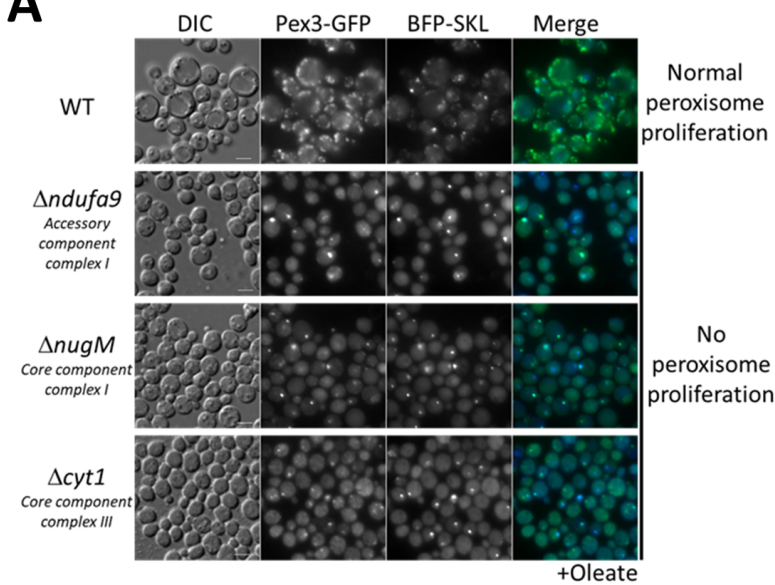
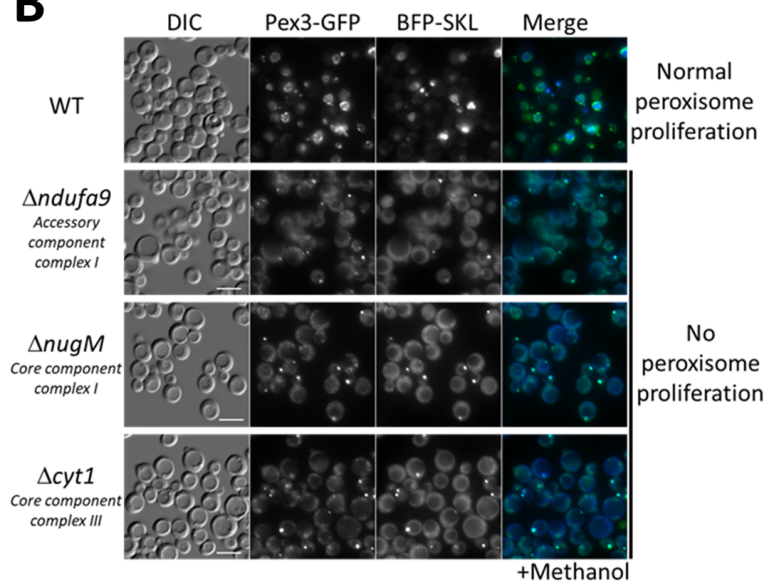
1134 107. Rao X, Huang X, Zhou Z, Lin X (2013) An improvement of the  $2^{(-\Delta\Delta CT)}$  method for  
1135 quantitative real-time polymerase chain reaction data analysis. *Biostat Bioinforma Biomath* **3**:  
1136 71-85  
1137

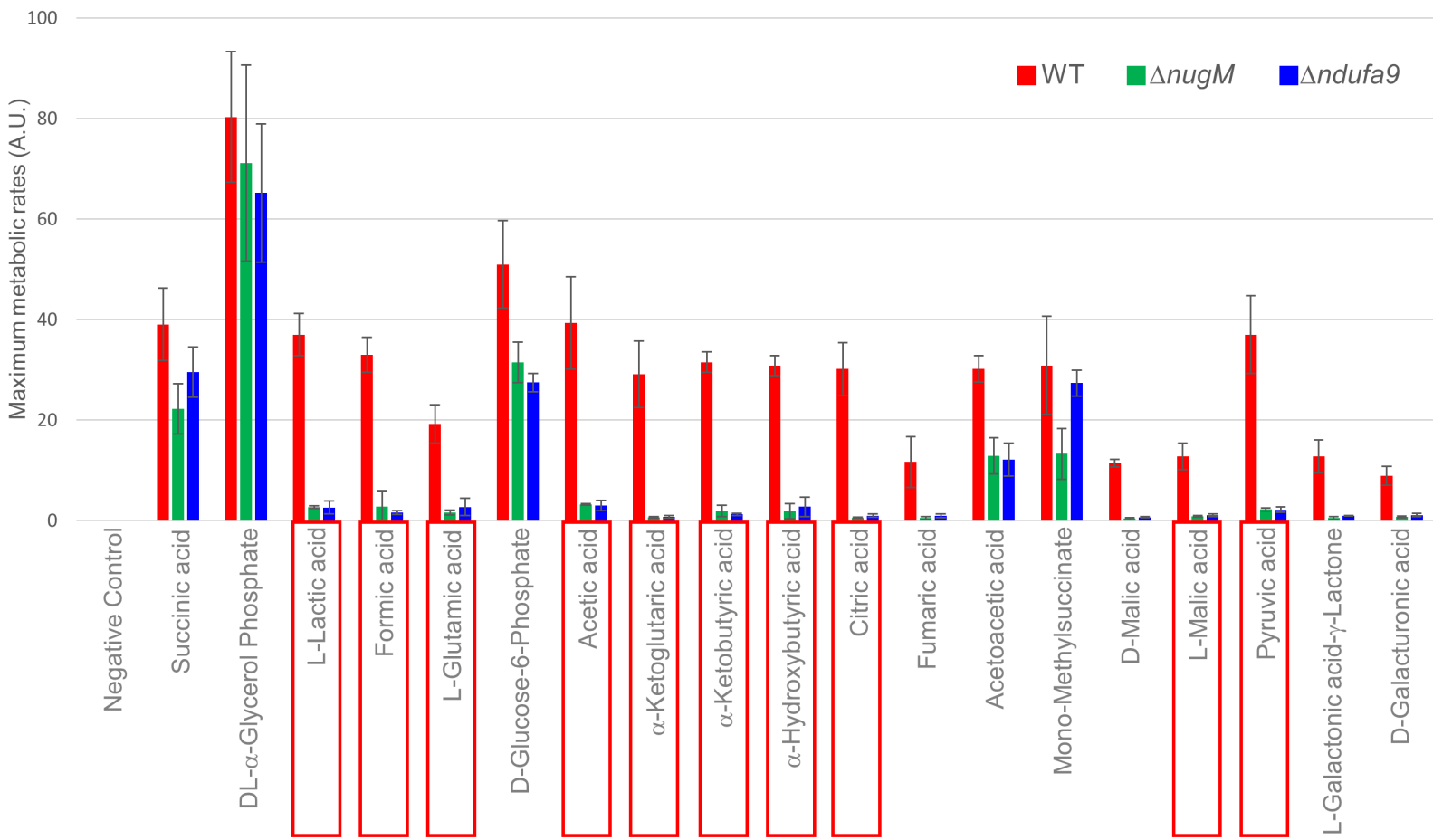


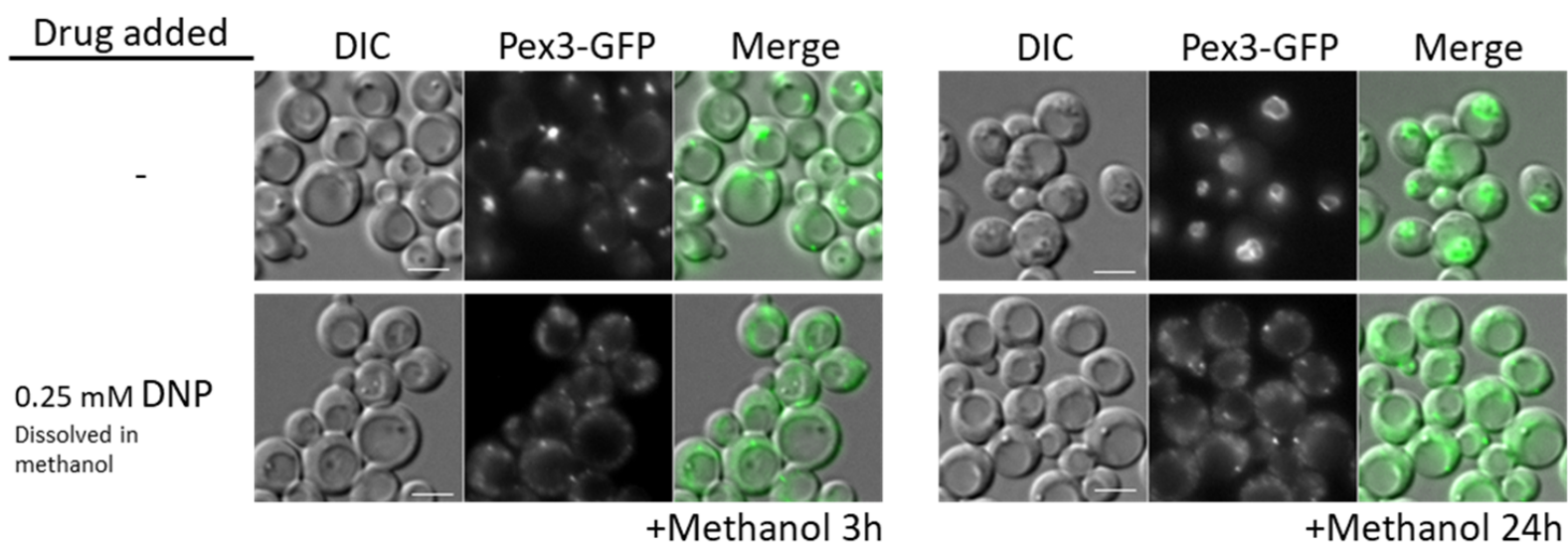
**A****B**





**A****B**

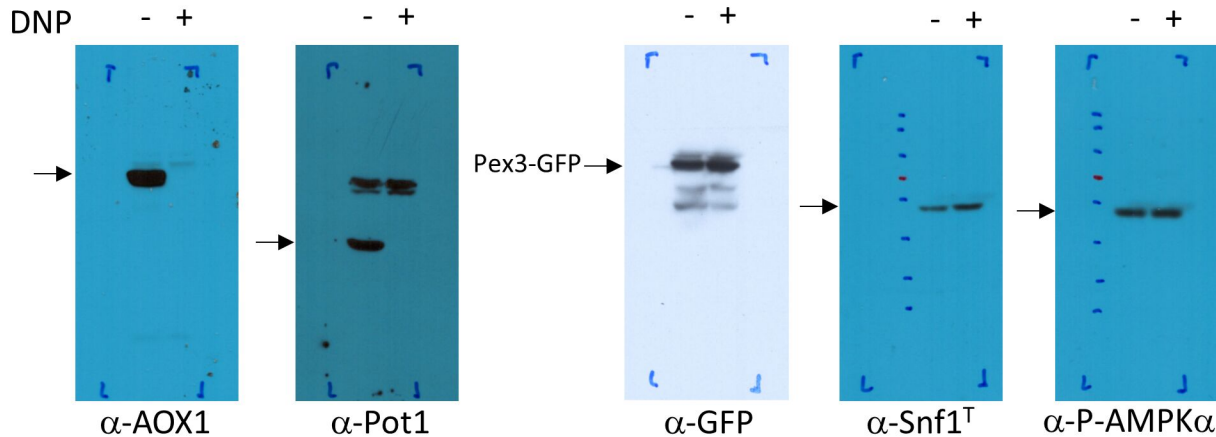
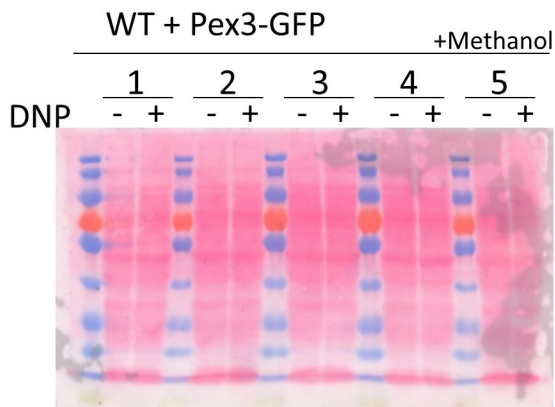




**A**

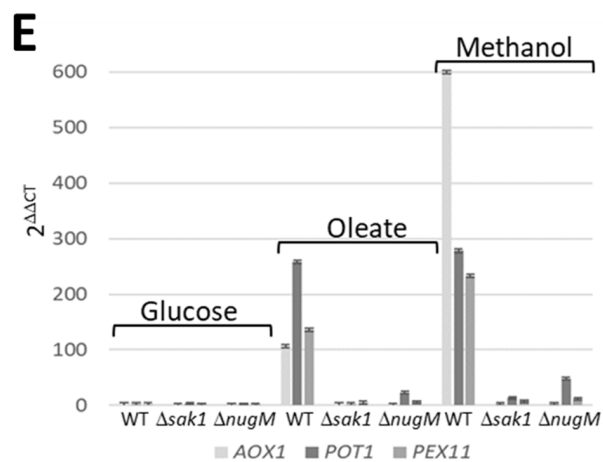
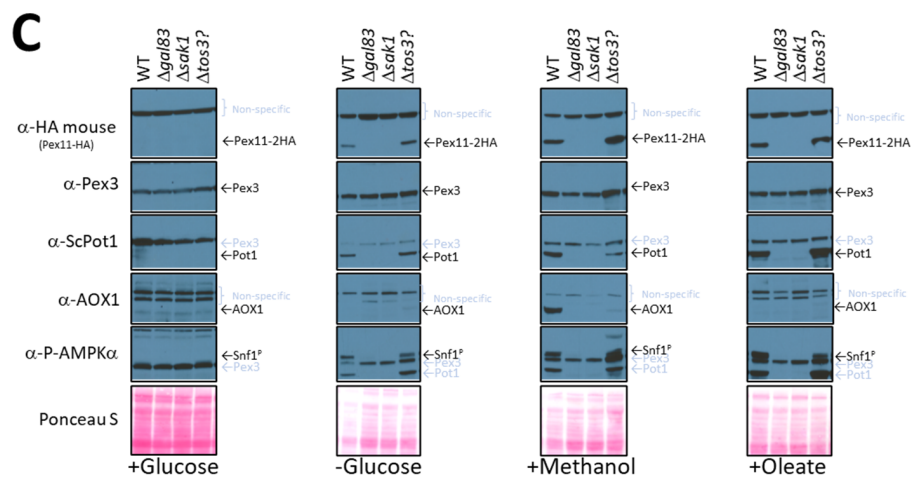
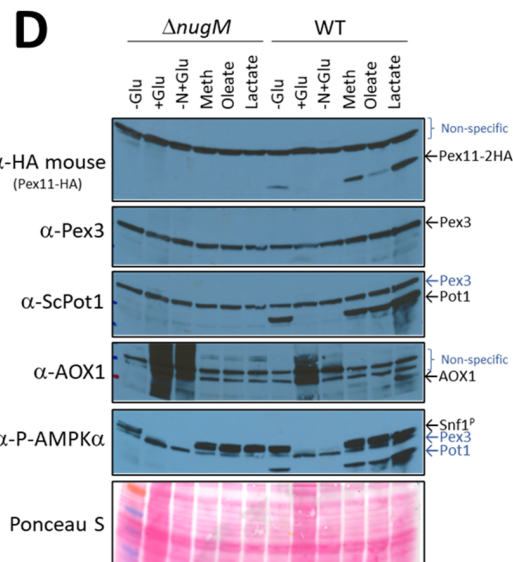
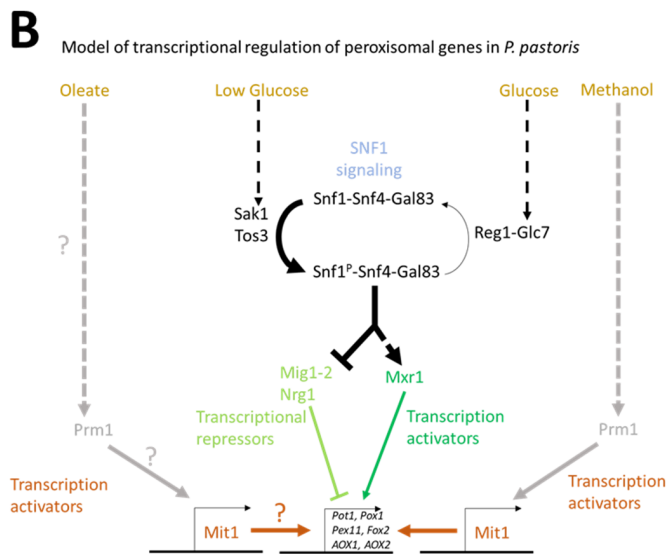
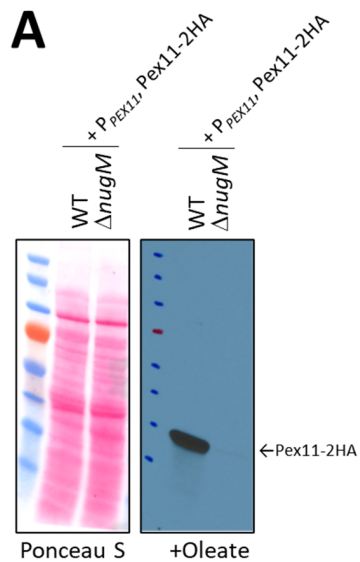
WT + Pex3-GFP

+Methanol

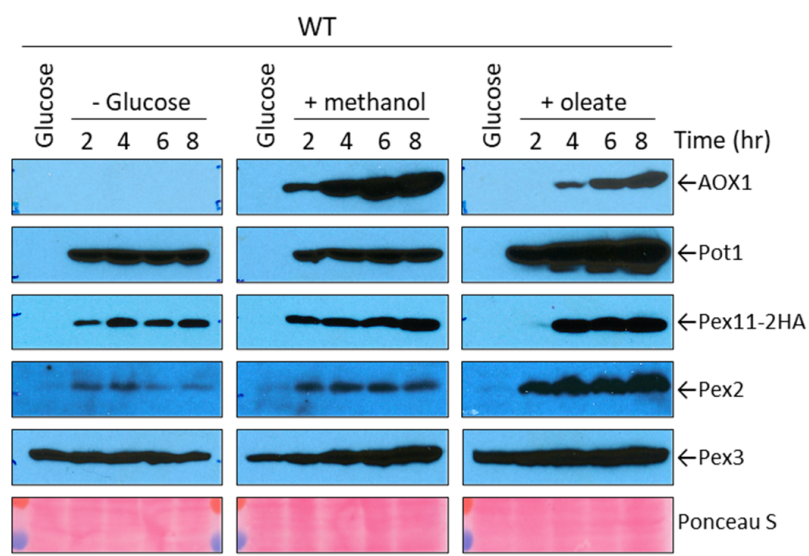
**B**

1. α-Snf1<sup>T</sup>
2. α-AOX1
3. α-Pot1
4. α-P-AMPKα
5. α-GFP

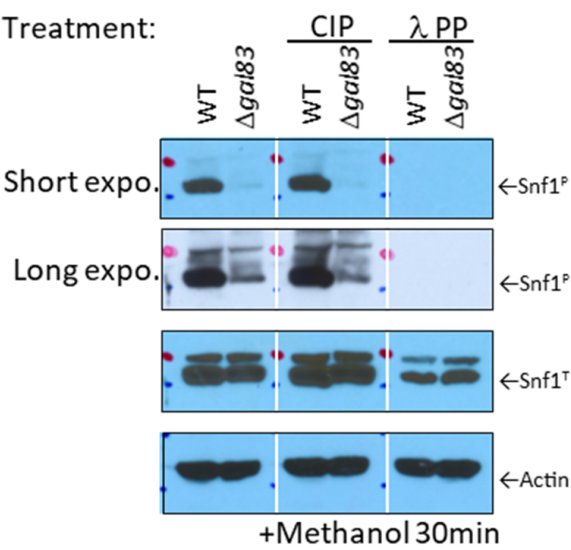




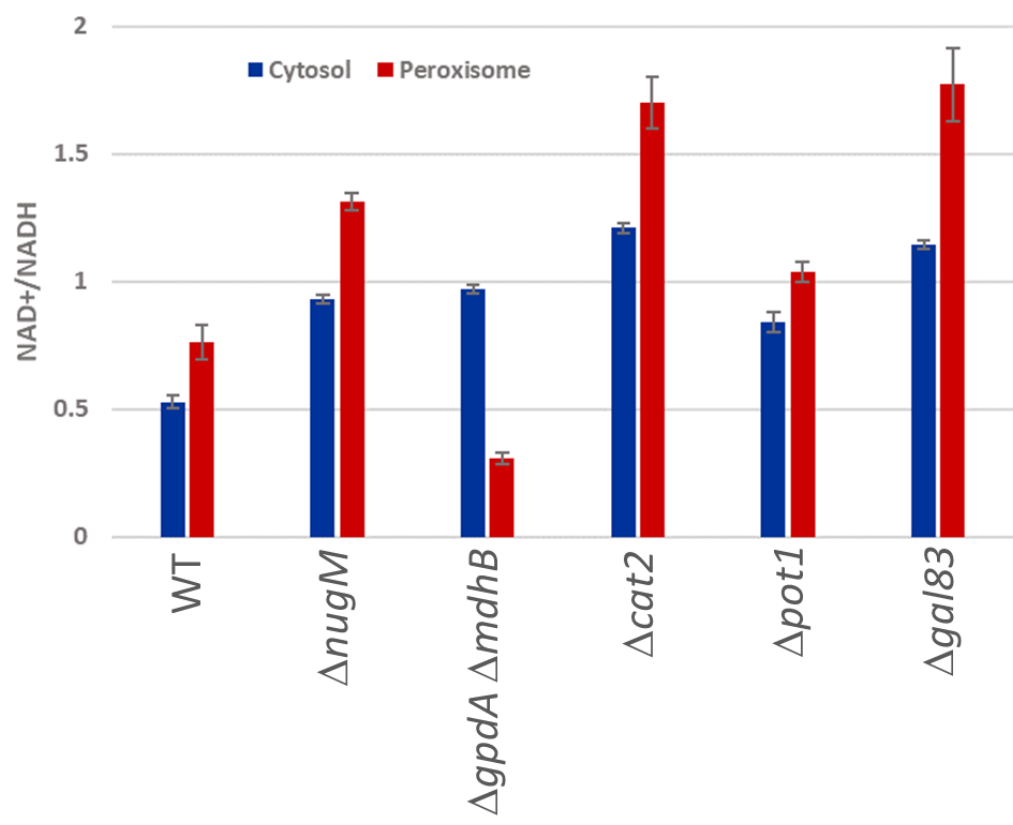
**A**



**B**

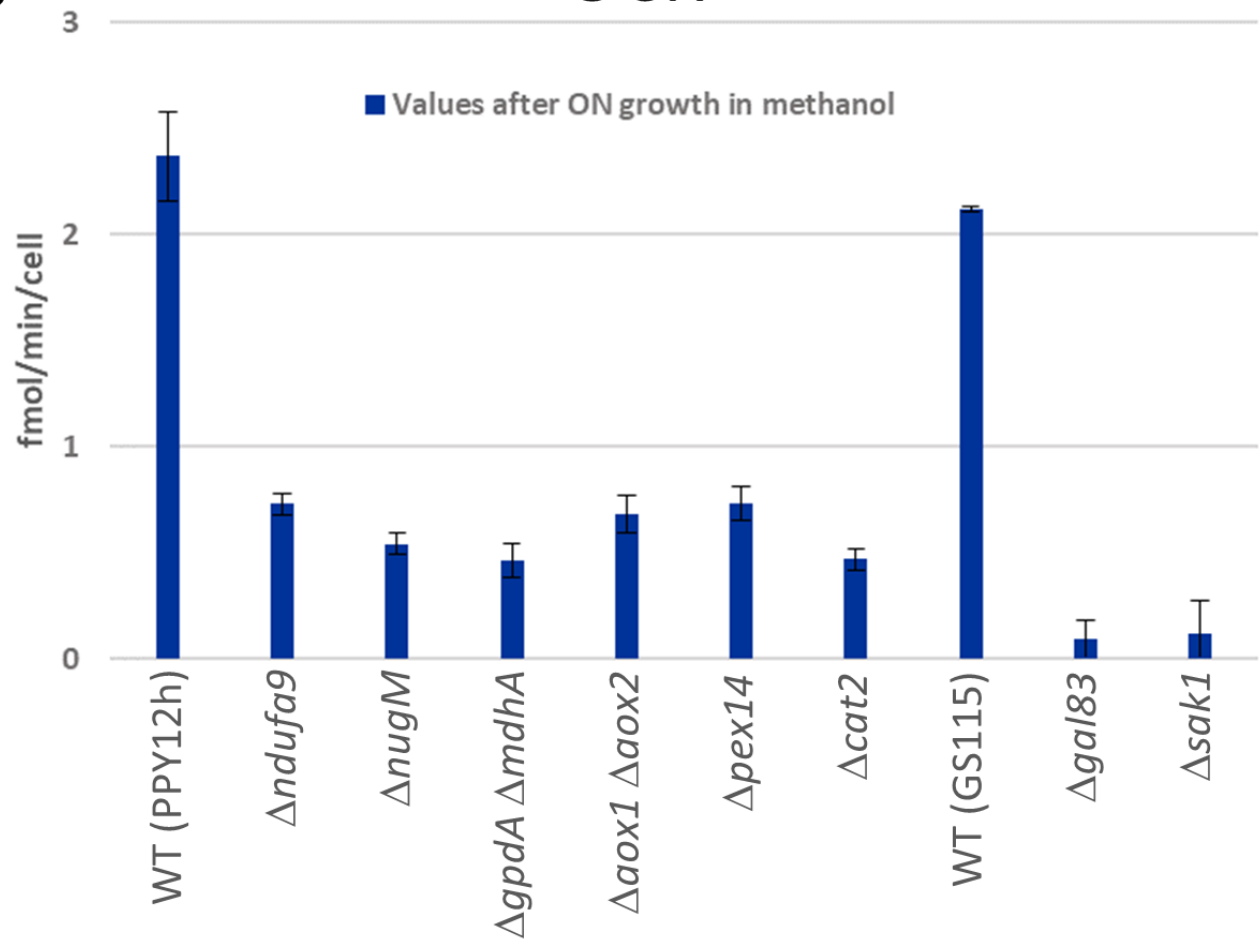


A

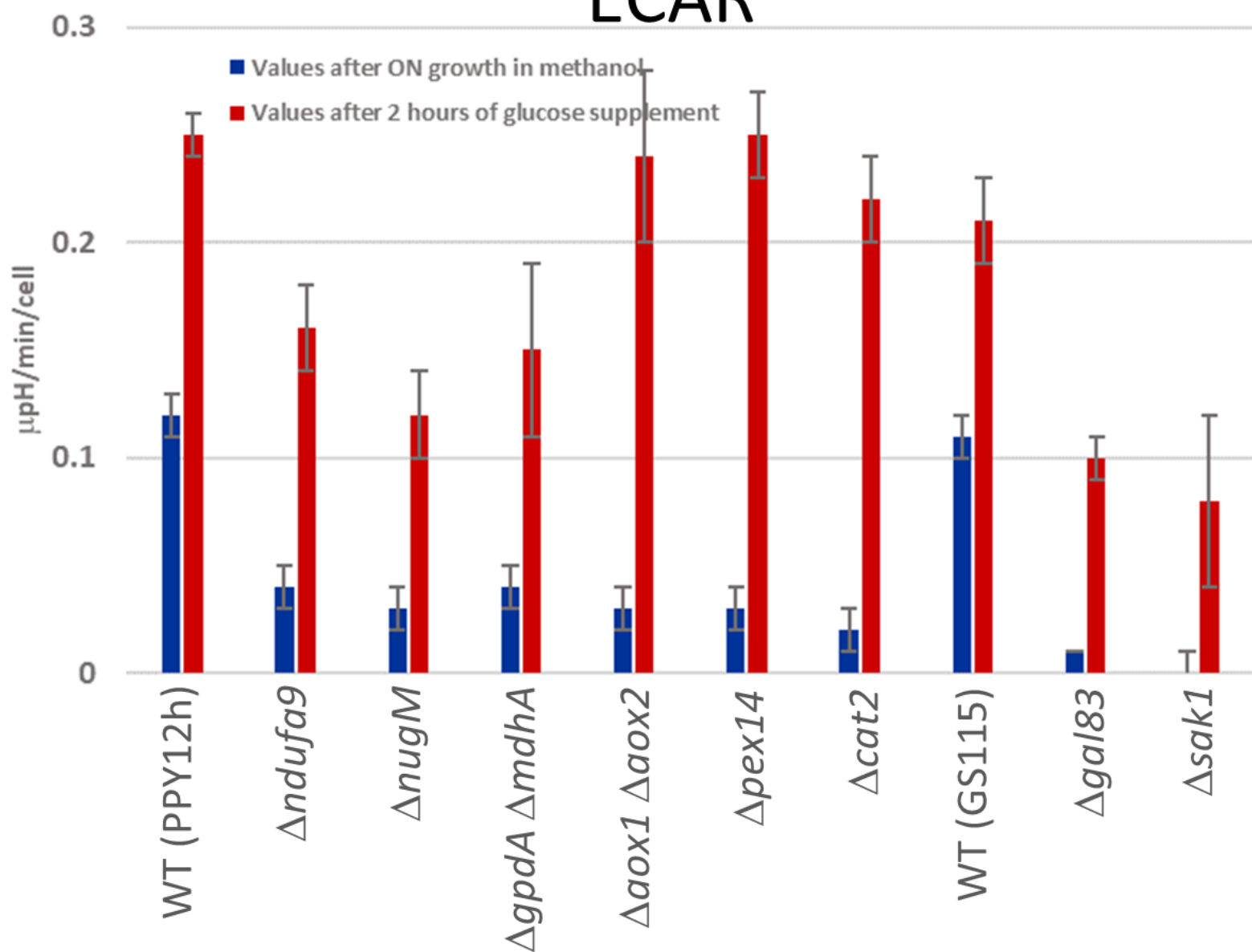


B

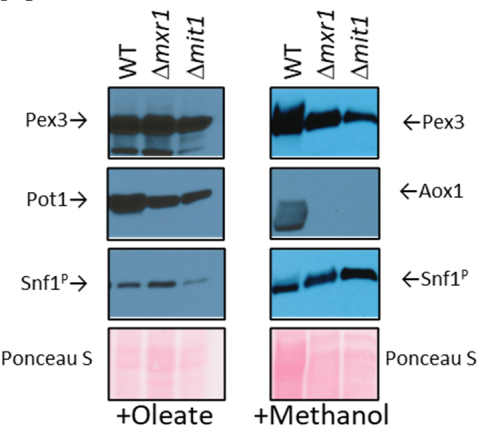
OCR



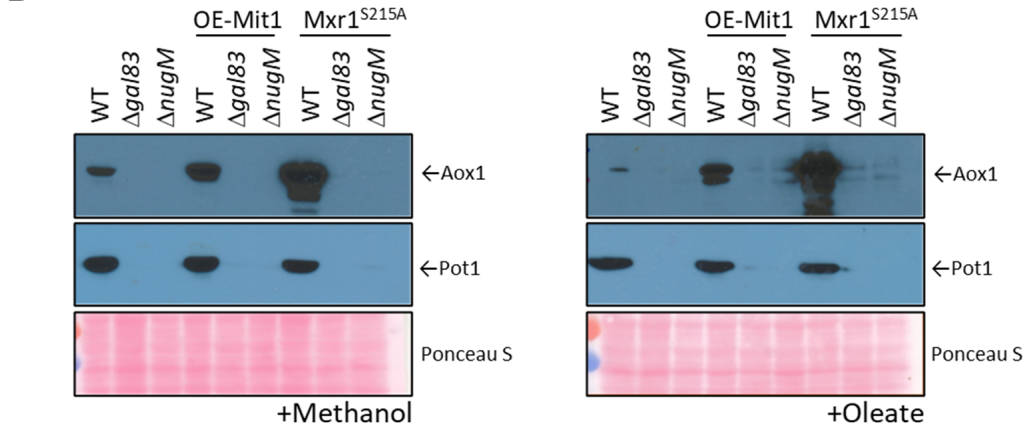
# ECAR

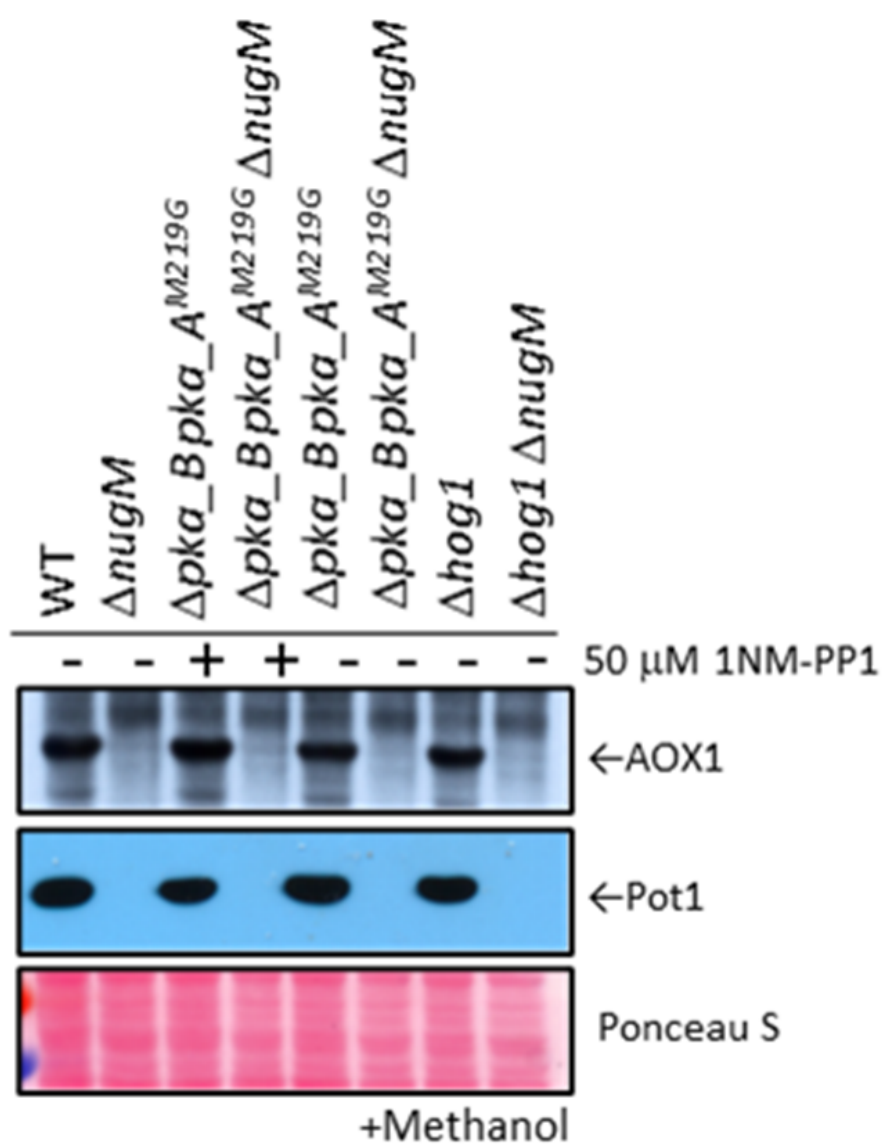
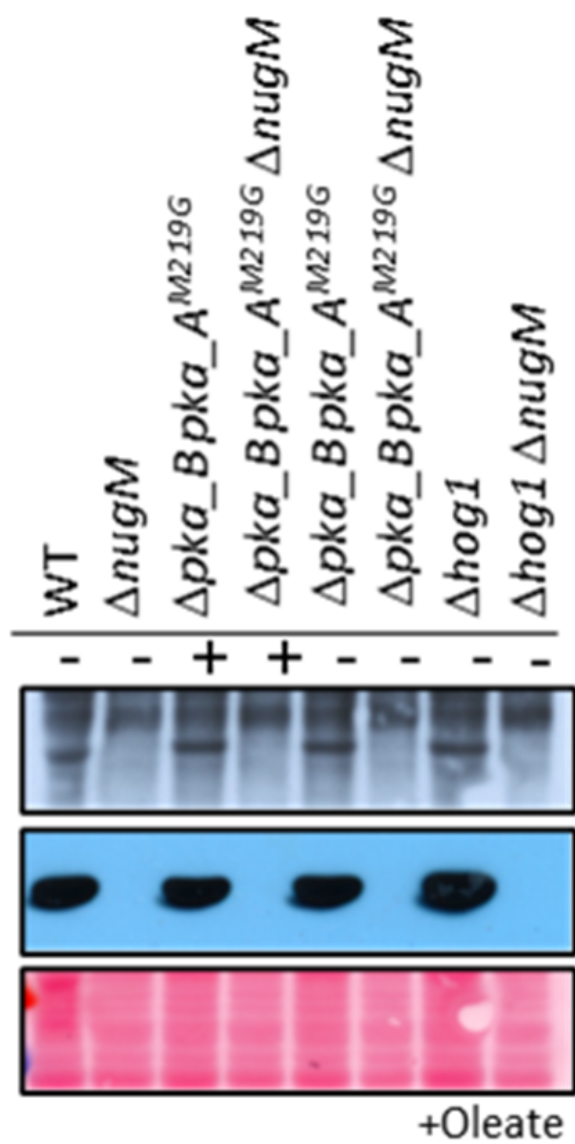


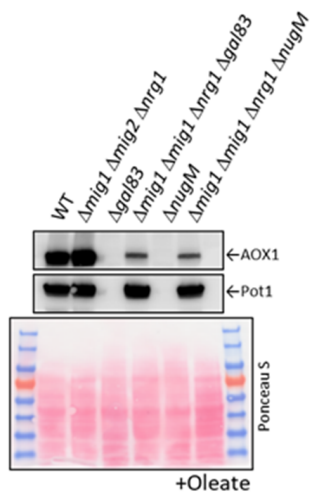
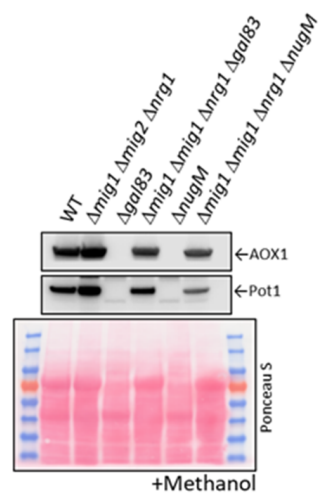
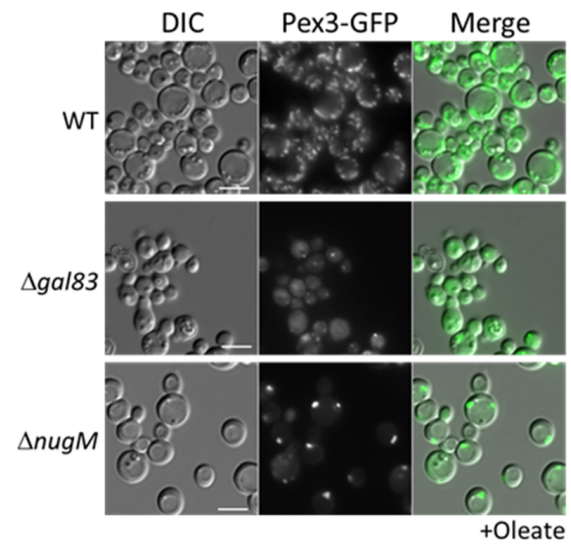
**A**



**B**





**A****B****C****D**